Michigan State University

National Superconducting Cyclotron Laboratory

# EMISSION TEMPERATURES FROM WIDELY SEPARATED STATES IN $^{14}$N- AND $^{129}$Xe-INDUCED REACTIONS

C. SCHWARZ, W.G. GONG, N. CARLIN, C.K. GELBKE, Y.D. KIM, W.G. LYNCH, T. MURAKAMI, G. POGGI, R.T. de SOUZA, M.B. TSANG, H.M. XU, D.E. FIELDS, K. KWIATKOWSKI, V.E. VIOLA, Jr. and S.J. YENNELLO

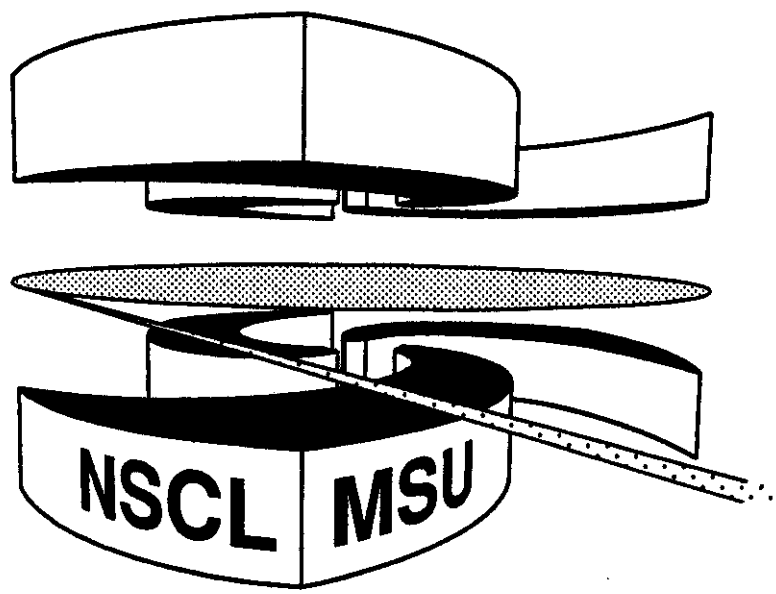


MSUCL-885

MARCH 1993

MSUCL-884 885
March, 1993

# Emission temperatures from widely separated states in $^{14}$N- and $^{129}$Xe-induced reactions.

C. Schwarz, W.G. Gong*, N. Carlin†, C.K. Gelbke,
Y.D. Kim‡, W.G. Lynch, T. Murakami§, G. Poggi**,
R.T. de Souza††, M.B. Tsang, and H.M. Xu‡‡
*National Superconducting Cyclotron Laboratory*
*and Department of Physics and Astronomy,*
*Michigan State University, East Lansing, Michigan 48824, USA*

D.E. Fields§§, K. Kwiatkowski, V.E. Viola, Jr.,
and S.J. Yennello‡‡
*Department of Chemistry and Indiana University Cyclotron Facility,*
*Indiana University, Bloomington, Indiana 47405, USA*

## Abstract

Charged-particle correlations were measured for the reactions $^{14}$N+$^{197}$Au and $^{14}$N+$^{27}$Al at E/A=75 MeV and for $^{129}$Xe+$^{27}$Al and $^{129}$Xe+$^{122}$Sn at E/A=31 MeV. Relative populations of widely separated states in $^{4}$He, $^{5}$Li, and $^{8}$Be, only weakly affected by side feeding, indicate emission temperatures of T=4-5 MeV for the $^{14}$N-induced reactions and values about 1 MeV lower for the $^{129}$Xe-induced reactions.

PACS numbers: 25.70.Mn, 25.70.Gh

## I. INTRODUCTION

Highly excited nuclear matter can be formed in intermediate energy heavy ion reactions. To address questions concerning the statistical properties of hot nuclei, it is important to determine their temperature. Experimental investigations have found evidence for a saturation in emission temperatures for fragments of $T = 4 - 6$ MeV [1–27] and evidence for a possible limitation on excitation energy of targetlike residues [28–42]. However, it is not clear if this saturation of excitation energy arises from an instability of bulk nuclear matter which may be related to a phase transition or from dynamical limitations which may govern the energy dissipation into internal degrees of freedom. Both statistical [43,44] and dynamical [45,46] models predict that nuclear matter at sufficiently high temperatures expands due to the action of thermal pressure. The rate of this expansion and the temperature at which fragments freeze out may depend on the nuclear equation of state [44,45]. In dynamical simulations little sensitivity of the energy deposition to the in-medium nucleon-nucleon cross section [45] is predicted. In statistical models, emission temperatures of bound systems appear to be related to the bulk instability of nuclear matter at low density and high temperature. In microcanonical models [43,47,48] this instability is manifested by the creation of new surfaces between hot fragments separating as the nuclear system undergoes a "cracking" phase transition at a characteristic cracking temperature of about 5 MeV. In another [44] model this instability is manifested by a rapid massive fragment formation during which the system remains at a constant temperature of about 5 MeV.

Until now, the relative populations of widely separated particle-unbound states have mainly been measured at forward angles for relatively light projectiles on heavy targets where contributions from the early nonequilibrated stages of the reaction predominate [8,10,12–15,18,20,27]. At such angles, the slopes of inclusive particle-energy spectra show "kinetic" temperatures of about 15-20 MeV [10,13] in the same reactions where the populations of excited states correspond to "emission" temperatures of about 3-5 MeV. Many explanations for these discrepancies have been offered [13,16,18,44,46,49]. Temperatures

extracted from energy spectra for non-compound emission mechanism are likely to be misleading, however, because of their sensitivity to Coulomb barrier fluctuations [50], sequential feeding from higher lying states, and dynamical effects such as collective motion [49,51–58] and non-equilibrium emission [59,60]. Sequential decay [5,18,61] and non-equilibrium phenomena can also influence the excited state population [17–19,45,46]. One must therefore extend the limited data base upon which our present understanding is based. In this respect, it is interesting to extend emission temperature measurements to a variety of entrance channel mass asymmetries. For comparisons with other observables that may be sensitive to the properties of an equilibrated residue and for comparisons with BUU predictions of the residue temperatures, measurements of emission temperatures at backward angles in normal kinematics are needed. Such measurements are, at present, scarce, and the relationship between the temperature for a hot equilibrated residue and the emission temperatures of fragments emitted from that residue has not been adequately explored.

In this paper, we report measurements of relative populations of widely separated states in $^{4}$He, $^{5}$Li, and $^{8}$Be nuclei for $^{14}$N+$^{27}$Al and $^{14}$N+$^{197}$Au collisions at E/A=75 MeV and for $^{129}$Xe+$^{27}$Al and $^{129}$Xe+$^{122}$Sn collisions at E/A=31 MeV using the same detector geometry. Reactions induced by $^{14}$N projectiles give rise to large contributions from the early nonequilibrated stages of the reactions and should, hence, be compared to previous measurements. For the $^{129}$Xe+$^{27}$Al reaction, emission from nearly equilibrated composite systems dominates and the extraction of unbound state populations will provide a test case for emission temperatures from equilibrated systems. The breakup scenario for $^{129}$Xe+$^{122}$Sn reactions is, at present, unknown. The present data may provide constraints on the scope of future measurements of symmetric collisions between heavy ions.

## II. EXPERIMENTAL DETAILS

The experiment was performed using $^{14}$N and $^{129}$Xe beams of E/A=75 MeV and of 31 MeV, respectively, extracted from the K1200 cyclotron of the NSCL: the beam intensities

were $5 \times 10^9$ and $1 \times 10^8$ ions per second, respectively. For the $^{14}$N beam we used $^{27}$Al and $^{197}$Au targets of areal densities 15 mg/cm$^2$ and 15.9 mg/cm$^2$, respectively, and for the $^{129}$Xe beam we used $^{27}$Al and $^{122}$Sn targets of areal densities 5.6 mg/cm$^2$ and 5.3 mg/cm$^2$, respectively. Light charged particles were detected with two $\Delta$E-E detector arrays, consisting of 300-400 $\mu$m thick silicon $\Delta$E-detectors and 10 cm long CsI(Tl) or NaI(Tl) E-detectors.

The first array consisted of 37 Si-CsI(Tl) [62] telescopes and was centered at polar and azimuthal angles of $\Theta = 25^0$ and $\Phi = 0^0$. Each telescope had a solid angle of $\Delta\Omega = 0.37$ msr, and the angular spacing between adjacent telescopes was $\Delta\theta = 2.6^0$. Isotopic identification was achieved for hydrogen through beryllium isotopes. The software energy thresholds for p, d, t, $^3$He, $^4$He, $^6$He, $^6$Li, $^7$Li, $^8$Li, $^9$Li, $^7$Be, $^9$Be, $^{10}$Be and $^{10}$B were 10, 12, 15, 30, 35, 40, 60, 65, 70, 80, 90, 100, 110, and 130 MeV, respectively.

The second array, consisting of 13 Si-NaI(Tl) telescopes, was centered at $\Theta = 25^0$ and $\Phi = 90^0$. Each telescope in this array covered a solid angle of $\Delta\Omega = 0.5$ msr, and the angular spacing between adjacent telescopes was $\Delta\theta = 4.4^0$. Isotopically identified p, d, t, $^3$He, $^4$He, $^6$He, $^6$Li, and $^7$Li particles were detected with energy thresholds of 12, 14, 16, 35, 40, 45, 80, and 90 MeV, respectively.

Coincidence and downscaled singles data were taken simultaneously. All data were corrected for random coincidences. Energy calibrations for individual detectors were obtained by elastically scattering $\alpha$-particles of 90, 116, and 160 MeV incident energy from a $(CH_2)_n$ target and detecting both the elastically scattered $\alpha$ -particles and the recoil protons at various laboratory angles. This provided energy calibrations with an accuracy of about 2% for p, d, t, $^3$He, and $^4$He. Heavier particles are calibrated by calculating the energy loss in the corresponding silicon $\Delta$E detector. This resulted in calibrations with accuracies of about 4% for lithium and 9% for boron; these calibration accuracies were assessed by comparing peak widths of experimental and calculated correlation functions (see Section IV B). For more details see Ref. [63].

## III. INCLUSIVE SPECTRA

Examples of inclusive energy spectra for $^4$He, $^6$Li, and $^7$Be, detected at $\Theta_{lab} = 18^0$, $25^0$, and $33^0$, are shown in Figs. 1-3. Spectra for reactions induced by $^{14}$N and $^{129}$Xe projectiles are shown in the top and bottom panels, respectively. To determine appropriate input for Monte-Carlo efficiency calculations, the yields for $^{14}$N-induced reactions were fitted with a simple three-source parameterization similar to that adopted in Ref. [64]:

$$\frac{d^2\sigma}{d\Omega/dE} = \sum_{i=1}^{3} N_i \sqrt{E - U_C}\; e^{-[E-U_C+E_i-2\sqrt{E_i(E-U_C)}\cos\Theta]/T_i}. \qquad (1)$$

Here, $N_i$, $T_i$, and $\Theta$ are the relative normalization, the kinetic temperature parameter, and the azimuthal angle, respectively. The energy $E_i$ is the laboratory kinetic energy of a particle which is stationary in the rest frame of the $i$th source. The Coulomb energy $U_C$ corrects for the Coulomb repulsion from heavy reaction residues, which are assumed to be at rest in the laboratory system.

For $^{129}$Xe-induced reactions, a constant Coulomb correction $U_C$ (as in Eq. 1) cannot be applied in the laboratory frame because the reaction residues have a large velocity in the laboratory rest frame. This issue is important because our measurements include particles with energies near the projectile and compound nucleus Coulomb barriers. To achieve a reasonable reproduction of the measured spectra, we employed a two-source parameterization [65]:

$$\frac{d^2\sigma}{d\Omega/dE} = \sum_{i=1}^{2} N_i \int_{U_1}^{U_2} dU \frac{(\exp -(U-U_C)^2/2\Delta_C^2)}{\Delta_C\sqrt{2\pi}} \sqrt{E(1-U/E_{cm,i})} e^{-(E_{cm,i}-U)/T_i}, \qquad (2)$$

which incorporates a Gaussian weighted smoothing of the Coulomb barrier of a source which is determined in a frame moving with the velocity of that source. In Eq. 2, $U_C$ and $\Delta_C$ are the mean and the standart deviation, respectively, and $E_{cm,i} = E + E_i - 2\sqrt{E_i E}\cos\Theta$ where $E_i$ is the kinetic energy of a particle at rest in source $i$. The integration limits were chosen as $U_1 = \max(0, U_C - 5\Delta_C)$ and $U_2 = \min(E_{cm,i}, U_C + 5\Delta_C)$. Fit parameters used for the description of the single fragment cross sections are shown in Tab. I. It must be stressed that

the extracted source parameters are not uniquely determined due to the small angular range covered by our detector array. One has also to be cautious about the physical interpretation of the source temperatures because such parameters are known to be sensitive to collective motion.

## IV. TWO-PARTICLE CORRELATION FUNCTIONS

### A. Background subtraction

Products from the decay of particle-unstable nuclei were detected as coincident particles and relative momentum spectra $Y_{tot}(q)$ were accumulated. The coincidence yield can be decomposed into two parts,

$$Y_{tot}(q) = Y_c(q) + Y_{back}(q), \tag{3}$$

where $Y_c(q)$ results from the decay of particle-unbound states of excitation energy, $E^* = q^2/(2\mu) + Q$ ($\mu$: reduced mass, Q: Q-value). The background yield $Y_{back}(q)$ results from coincident particles emitted independently; it is largely determined by the available phase space. To remove the effects of detector thresholds and finite angular coverage, which influence $Y_C$ and $Y_B$ in similar fashion, we constructed the correlation function [10]

$$[1 + R(q)]_{tot} = \frac{Y_{tot}(q)}{C_{12}\sigma_1\sigma_2} \tag{4}$$

from the inclusive particle yields $\sigma_1$, $\sigma_2$. The normalization constant $C_{12}$ is determined from the requirement that $[1 + R(q)]_{tot} = 1$ for large values of $q$ at which no particle unstable decays contribute. At small relative momenta there is a minimum in the correlation function due to the Coulomb final state interaction between the two coincident particles. To account for this Coulomb minimum, we have parameterized the background correlation function as

$$[1 + R(q)]_{back} = 1 - e^{(\frac{q^2/2\mu}{\Delta_b})^d}. \tag{5}$$

Here, the parameters $\Delta_b$ and $d$ govern the width of the minimum at $q = 0$.

For our data analysis, we determined the sensitivity of the extracted coincidence yield $Y_c$ to uncertainities of the background by choosing two extreme assumptions for this background. These two choices of background are indicated by dashed curves in Figs. 4-8. For a given background, the yield of particle pairs due to sequential decay was extracted as

$$Y_c(q) = Y_{tot}(q) - C_{12}\sigma_1\sigma_2[1 + R(q)]_{back}. \tag{6}$$

### B. Population of states

Information about relative populations of states are obtained from the relative decay yields. The coincidence yield, $Y_c(E^*)$, resulting from the decay of particle-unstable states can be approximated by [10]

$$Y_c(E^*) = N \int dE \epsilon_c(E^*, E) \frac{dn(E)}{dE}, \tag{7}$$

where N is a normalization constant; $dn(E)/dE$ is the decay spectrum; $\epsilon_c(E^*, E)$ is the efficiency of the experimental apparatus for the detection of particle pairs resulting from the decay of specific particle-unstable nuclei and E and $E^*$ denote the actual and measured excitation energies, respectively. For narrow, thermally populated states, the decay spectrum can be expressed as

$$\frac{dn(E)}{dE} = e^{-E/T} \sum_i \frac{(2J_i + 1)\Gamma_i/2\pi}{(E - E_i)^2 + \Gamma_i^2/4} \frac{\Gamma_{c,i}}{\Gamma_i}. \tag{8}$$

In in Eq. 8, $\Gamma_{c,i}/\Gamma_i$ is the branching ratio for the decay of state $i$ into the channel $c$, and T is the emission temperature.

The efficiency function is obtained from Monte-Carlo simulations, which take into account the kinetic energy spectra of the particle-unstable fragments, as well as the precise geometry and detector response and the angular straggling in the target [10]. Wherever possible, the kinetic energy spectrum for the particle-unstable fragments is assumed to be the same as the energy spectrum of the stable nuclei of the same isotope. For $^5$Li or $^8$Be, where there are no particle stable states, the energy spectra were assumed to be the same

as for $^{6}$Li and $^{7}$Be fragments, respectively. The emission temperature T is extracted by comparing the calculated yields from the decay of two widely separated particle-unbound states with the experimental yields. The comparison can also involve the yield of particle stable states $i$ of the parent nucleus, which is given by

$$Y_{stable} = N\epsilon\sum_{i}(2J_i + 1). \tag{9}$$

Here, $\epsilon$ denotes the (singles) efficiency for detecting the stable fragments.

For broad states, the assumption of constant decay width, $\Gamma_C$, is not valid because penetrability effects have to be taken into account and the Breit-Wigner expression in Eq. 8 is not justified. For such states we used a one-level R-matrix formalism [66]. Here, the formal width of the level, $\Gamma_i = 2P_{li}\gamma_i^2$, and the resonance energy, $E_i = E_R + \Delta_{li}$, are functions of the excitation energy E. Their energy dependence is expressed in terms of the penetrability $P_{li}$ and shift function $\Delta_{li}$ for the relative angular momentum $l$ between the particles. The parameters for the R-matrix formalism are taken from the literature [67–70].

Large distortions of the resonance-line shape can occur when fragments with different charge to mass ratios are accelerated in the Coulomb field of a heavy residue. Dependent on the geometrical decay configuration, this Coulomb distortion may increase or decrease the relative momenta [71]. Such effects have been explored previously for the case of p-$\alpha$ correlations resulting from the decay of the ground state of $^{5}$Li ($\Gamma_{c.m.} = 1.5$) [72]. Integrating over the relative momentum distributions of the experimental and calculated peaks (Eq. 7) reduces the uncertainty of extracting the resonance yield.

### C. Experimental correlation functions

In this subsection we present the two-particle correlation functions measured in this experiment. These correlation functions were normalized at the relative momenta given in Table II. Aside from the detector energy thresholds, discussed in section II, no further constraints on the data were applied. Fig. 4 shows the correlation functions for p-t pairs. (Note

the different vertical scales for the $^{14}$N- and $^{129}$Xe-induced reactions!) The first maximum corresponds to the $J^{\pi} = 0^{+}$ state in $^{4}$He at 20.21 MeV ($\Gamma_{c.m.} = 0.5$, $\Gamma_p/\Gamma = 1.00$, the second is due to the two overlapping $J^{\pi} = 0^{-}$ and $2^{-}$ states at 21.0 MeV and 21.8 MeV ($\Gamma_{c.m.} = 0.84$, $\Gamma_p/\Gamma = 0.76$ and $\Gamma_{c.m.} = 2.01$, $\Gamma_p/\Gamma = 0.76$, respectively) [73]. Due to the folding of the decay yield with the detector efficiency (Eq. 7), the peaks are slightly shifted to lower relative momenta, as compared to the exact locations of the states in $^{4}$He at $q = 23, 41, 53$ MeV/c. The magnitudes of the peaks of the correlation functions are much smaller for $^{129}$Xe-induced reactions than for $^{14}$N-induced reactions, suggesting a significantly larger space time extent for $^{129}$Xe-induced reactions than for $^{14}$N-induced reactions [65]. These correlation functions also exhibit a shift of the second peak to lower relative momenta by $\Delta q \approx 10$ MeV/c. This shift may be induced by three body Coulomb distortions caused by heavily charged reaction residues.

The dashed lines in Fig. 4 depict two extreme assumptions for the background correlation functions calculated by Eqs. 1 and 2. The minimum background correlation function was found by requiring that the peaks in the yields still look reasonable. The solid curves show correlation functions calculated for a background correlation function which is intermediate between the extremes shown by the dashed curves. In these calculations the individual states were assumed to be thermally populated and the overall normalization N was normalized to the data. Because of the width of the states and proximity to the decay threshold, an R-matrix parameterization was taken [67]. The calculated curves agree well with $^{14}$N data. For $^{129}$Xe-induced reactions, the location of the second peak is not well described.

The $p - \alpha$ correlation functions, shown in Fig. 5, exhibit two maxima. The broad maximum at $q \approx 50$ MeV/c corresponds to the decay of the "ground state" of $^{5}$Li ($J^{\pi} = 3/2^{-}$, $\Gamma_{c.m.} = 1.5$, $\Gamma_p/\Gamma = 1.00$ [72]). The peak at $q \approx 15$ MeV/c is due to the three-body decay $^{9}B \rightarrow 2\alpha + p$ [71]. For the calculation of the efficiency function, the parent $^{5}$Li distribution was parameterized with Eqs. 1,2 using the source parameters extracted for $^{6}$Li. This assumption was motivated by the work of Chen et al. [12] who have shown that uncertainties due to the unknown energy spectra of the particle-unstable parent nuclei are

much smaller than the uncertainities due to different assumptions regarding the background.

Similar to the p-t correlation, the $^5$Li "ground state" peak for the $^{129}$Xe-induced reactions is about 8-10 times lower than for the $^{14}$N-induced reactions. In both cases, the line shape of the $^5$Li ground state is distorted by the presence of the emitting source described by Eq. 8. This distortion must be considered in the analysis. The solid lines in Fig. 5 show calculations for the $^{14}$N-induced reactions assuming $T = 4$ MeV and for the $^{129}$Xe-induced reactions assuming $T = 3$ MeV, respectively. The R-matrix parameters were taken from Stammbach et al. [68]. The resonance energy for the calculated $3/2^-$ state was shifted to lower relative energy by 200 keV an effect which may be caused by 3-body Coulomb distortions caused by target-like residues [71]. Except for the case of $^{129}$Xe+$^{27}$Al, where the $^9$B decay is most significant, the curves in Fig. 5 agree very well with the data. For the yields given by the solid curves, the background was assumed to be given by the upper dashed curve in Fig. 5.

The largest peak in the d-$^3$He correlation, Fig. 6, originates from the 16.7 MeV state in $^5$Li ($J^\pi = 3/2^+$, $\Gamma_{c.m.} = 0.2$, $\Gamma_d/\Gamma = 0.86$ [72]). The R-matrix parameters were taken from Kunz et al. [69]. For the $^{14}$N-induced reactions one observes a broad maximum at $q \approx 90$ MeV/c which results from the decay of the $1/2^+$ state in $^5$Li. The region of the correlation function in the neighborhood of this peak was not fit because the R-matrix parameterization for this state is not known [69] (solid lines in Fig. 6). Because the correlation for the $^{129}$Xe-induced reactions is close to one, it can be described by $Y_C$=0 if one assumes the maximum background correlation function shown by the upper dashed curve. It can also be somewhat better described by a non-zero resonance yield depicted by calculated correlation function (solid curve) which assumes a background correlation function between the two extremes (depicted by the dashed lines).

Fig. 7 shows $\alpha - \alpha$ correlation functions. The peak at $q \approx 105$ MeV/c results from the decay of the 3.04 MeV state in $^8$Be ($J^\pi = 2^+$, $\Gamma_{c.m.} = 1.5$, $\Gamma_\alpha/\Gamma = 1.00$ [72]). For the present investigation, the structures at lower relative momenta are not of interest, for a detailed discussion see Ref. [10,70]. To improve the agreement between calculated line shapes (solid

lines in Fig. 7) and the data we have allowed the maximum background correlation shown as the upper dashed line, to exeed unity. For $^{129}$Xe-induced reactions the peaks of correlation function due to the $2^+$ state are only significantly smaller than for the $^{14}$N-induced reactions. For the calculation of the efficiency function, the $^8$Be parent distribution was assumed to be given by the parameters in Tab. I that were used to describe the $^7$Be cross sections shown in Fig 3.

The p-$^7$Li correlation functions are shown in Fig. 8. The first maximum at $q \approx 25$ MeV/c corresponds to the 17.64 MeV state in $^8$Be ($J^\pi = 1^+$, $\Gamma_{c.m.} = 10.7$ keV, $\Gamma_p/\Gamma = 1.00$ [72]), the second to the 18.15 MeV state ($J^\pi = 1^+$, $\Gamma_{c.m.} = 138$ keV). This state decays with $\Gamma_p/\Gamma = 0.04$ to the 0.48 MeV state in $^7$Li and with $\Gamma_p/\Gamma = 0.96$ to the ground state of $^7$Li [72]. The third peak consists of a group of states at 18.9 MeV ($J^\pi = 2^-$, $\Gamma_{c.m.} = 122$ keV, $\Gamma_p/\Gamma = 0.86$ [74]), 19.1 MeV ($J^\pi = 3^+$, $\Gamma_{c.m.} = 270$ keV, $\Gamma_p/\Gamma = 1.00$ [72]), 19.2 MeV ($J^\pi = 3^+$, $\Gamma_{c.m.} = 230$ keV, $\Gamma_p/\Gamma = 0.5$ [72]), 19.4 MeV ($J^\pi = 1^-$, $\Gamma_{c.m.} \approx 650$ keV, we assumed: $\Gamma_p/\Gamma = 0.5$ [72]), 19.9 MeV ($J^\pi = 4^+$, $\Gamma_{c.m.} = 700$ keV, $\Gamma_p/\Gamma = 0.04$ [72]). We could not describe all these states assuming a thermal population of excited states in $^8$Be and a background correlation function which increases monotonically with $q$ according Eq. 5. This may indicate a nonstatistical population of states. On the other hand structures could occur in the correlation function due to 3-body decays or decays to excited states in $^7$Li. To explore this as a possible upper limit of the experimental background, we have explored hand-drawn dashed lines, shown in Fig. 8 as extreme limits to the background.

## V. RESULTS

In general, sequential feeding from particle decays of heavier nuclei will influence the ratios of the yields of particle-unstable excited states for specific fragments. For ratios involving the particular excited states of $^4$He, $^5$Li, and $^8$Be discussed in this paper, detailed calculations have shown that they are rather insensitive to sequential feeding corrections. Therefore emission temperature can be described by comparing the experimental yields to

yields calculated by Eqs. 7 and 8. Figure 9 shows measured ratios of the p-t coincidence yield from the $J^\pi = 0^+$ state at 20.21 MeV to the measured particle stable yield of $^4$He. For this comparison, the yield from $J^\pi = 0^+$ state was integrated over the interval q=10-30 MeV/c. The calculated resonances, given by the solid curves in Fig. 4, were integrated over the same relative momentum range as in the data. Ratios calculated as function of the temperature parameter T are shown in Fig. 9 as solid lines. The uncertainties for the experimental ratios (shaded areas in Fig. 9) are given by the uncertainties in the subtraction of the background function of the measured p-t yields. (This uncertainty has been estimated from the dashed lines in Fig. 4). These bounds determine the corresponding uncertainties of the extracted temperatures. For the $^{14}$N-induced reactions, which are dominated by preequilibrium processes, apparent temperatures of T=4.8±0.3 MeV (T=4.7±0.3 MeV) for the $^{27}$Al ($^{197}$Au) target, respectively, were found. For the $^{129}$Xe-induced reactions, which are more sensitive to equilibrium emission mechanisms, distinctly lower apparent temperatures of T=3.1±0.2 MeV (T=3.5±0.3 MeV) for the $^{27}$Al ($^{122}$Sn) target, respectively, were observed. Lower temperatures, T=$2.2^{+0.3}_{-0.2}$ MeV, were measured by Dabrowski et al. [75] in $^{40}$Ar + Ag collisions at E/A=44 MeV for $^4$He fragments emitted at backward angles. This difference between our temperatures for the $^{122}$Sn target and those of Dabrowski et al. are surprising and not understood.

To obtain the population ratios for states in $^5$Li, we used the particle-unstable "ground state" ($J^\pi = 3/2^-$), which decays into p-$\alpha$ pairs, and integrated the p-$\alpha$ yield from q=25 MeV/c to q=100 MeV/c (Fig. 5). The yield of the high lying ($J^\pi = 3/2^+$) state at 16.7 MeV, which decays preferentially into d-$^3$He pairs, was integrated from q=10 MeV/c to q=60 MeV/c (Fig. 6). Ratios calculated as a function of emission temperature are shown in Figure 10 as solid lines. Again the $^{14}$N-induced reactions reveal higher temperatures than those with $^{129}$Xe as projectiles. For the latter only upper limits could be estimated because the d-$^3$He correlations (Fig. 6) were consistent with the maximum bound of the background correlation. Here, we found temperatures of $T = 3.9 \pm 0.3$ MeV ($T = 3.7 \pm 0.2$ MeV) for the $^{14}$N+$^{27}$Al ($^{14}$N+$^{197}$Au) reaction, and temperatures of $T \leq 3.0$ MeV ($T \leq 3.5$ MeV) for the

$^{129}$Xe+$^{27}$Al ($^{129}$Xe+$^{122}$Sn) reaction, respectively

Population ratios of widely separated states in $^{8}$Be fragments (Fig. 7, 8) give similar results. Here, we analysed the ratio between the ($J^{\pi} = 1^{+}$) state at 17.64 MeV, which decays in p and $^{7}$Li, and the ($J^{\pi} = 2^{+}$) state at 3.04 MeV, which decays into two $\alpha$-particles. Yields of the p-$^{7}$Li and $\alpha$-$\alpha$ decay channels were integrated from q=18 MeV/c to 32 MeV/c and from q=65 MeV/c to 160 MeV/c, respectively. Consistent with the results for $^{4}$He and $^{5}$Li fragments, higher temperatures are observed (Fig. 11) for $^{14}$N-induced reactions at the higher incident energy of E/A=75 MeV ($T = 4.9 \pm 0.9$ MeV for $^{14}$N+$^{27}$Al and $T = 4.5 \pm 0.9$ MeV for $^{14}$N+$^{197}$Au, respectively) and lower temperatures for $^{129}$Xe-induced reactions at the lower incident energy of E/A=31 MeV ($T = 3.3 \pm 0.5$ MeV for $^{129}$Xe+$^{27}$Al and $T = 3.9 \pm 1.0$ MeV for $^{129}$Xe+$^{122}$Sn, respectively).

A summary of all extracted emission temperatures is shown in Fig. 12. The uncertainties are due to extreme assumptions of the background correlation functions. Estimates of the range of emission temperatures consistent with these measurements are indicated by the dashed lines; for $^{129}$Xe-induced reactions the average was taken over the $^{4}$He and $^{8}$Be fragments. Emission temperatures from the states discussed in this paper are expected to be robust with respect to distortions due to sequential feeding from heavier particle-unstable nuclei for temperatures less than 5 MeV [61]. The largest distortions were predicted for $^{4}$He for which calculations at T=5 MeV predict populations corresponding to extracted temperatures which are about 0.5 MeV lower due to sequential decay.

The extracted temperatures fall into the established systematics for light projectiles impinging on heavier targets. Fig. 13 shows a comparision of the extracted temperatures for a variety of incident energies. The solid diamonds provide the results for normal kinematics (preequilibrium emission) and the solid circles provide the results for reverse kinematics (emission from target-like residues) obtained in the present work.

## VI. SUMMARY AND CONCLUSION

We have measured the relative populations of widely separated states in $^{4}$He, $^{5}$Li, and $^{8}$Be fragments. We studied $^{14}$N-induced reactions at E/A=75 MeV for which emission is dominated by the early non-equilibrated stages of the reaction and $^{129}$Xe-induced reactions at E/A=31 MeV for which emission is dominated by the later equilibrated stages of the reaction.

Average emission temperatures extracted from the relative populations of widely separated states are T=4.3±0.2 MeV for $^{14}$N+$^{27}$Al and T=4.1±0.2 MeV for $^{14}$N+$^{197}$Au. These values are significantly smaller than the values of "kinetic temperature" parameters (T≈18-20 MeV) which characterize the slopes of the kinetic energy spectra of protons emitted at $\theta_{lab}$ ≈25° [65]. The extracted emission temperatures are consistent with previous measurements (Fig. 13). Their low values may be related to cooling due to expansion [43,44,48], to preequilibrium effects, [20,45,55–58,76,77], or both.

Average emission temperatures extracted for the $^{129}$Xe-induced reactions were lower by about 1 MeV, T=3.1±0.2 MeV for $^{129}$Xe+$^{27}$Al and T=3.5±0.3 MeV for $^{129}$Xe+$^{122}$Sn (Fig. 12). For the $^{129}$Xe+$^{27}$Al reaction, these temperatures are slightly smaller than the kinetic temperature parameters T≈4-6 MeV which characterize the energy spectra for protons [65]. The same is true for the $^{129}$Xe+$^{122}$Sn reaction for which the extracted temperature is slightly smaller than the kinetic temperature (T≈4 MeV) which characterizes the emission of protons [65] from the projectile-like source which dominates emission at the angles of the present measurement. Previous investigations [78] have reported that the apparent temperatures of such spectra are considerably larger than the temperature of compound systems. These studies suggest that such backward angle proton spectra may still be contaminated by preequilibrium emission.

Within experimental errors, the emission temperatures extracted for the $^{129}$Xe-induced reactions are comparable (though slightly smaller in magnitude) to temperatures previously extracted from other reactions at comparable incident energies per nucleon in which large

nonequilibrium contributions could not be excluded (Fig. 13). For example, average emission temperatures of T=3-4 MeV were determined from the population of particle-unbound states of particles emitted at $\theta_{lab} \approx 38°$ in $^{14}N+^{nat}Ag$ reaction at E/A=35 MeV [18] and from the relative populations of particle-stable states in $^{32}S+^{nat}Ag$ and (and $\theta_{lab} \approx 20°$-$50°$) [5].

The emission temperatures determined for $^{129}Xe+^{27}Al$ are also smaller than temperatures expected for equilibrated fusion-like residues. Linear momentum transfer (LMT) systematics [79] predict a ratio of the linear momentum transfer to the initial beam momentum of $p_{||}/p_{beam} = 0.73$ and, as determined from an incomplete fusion scenario for the $^{129}Xe+^{27}Al$ reaction, an excitation energy of $E^*/A$=3.4 MeV. Assuming a level density parameter of $a=A/8$ $MeV^{-1}$, this provides a compound nucleus temperature of 5.2 MeV, which is significantly larger than the observed emission temperature. This estimate of excitation energy from an incomplete fusion ansatz is an upper limit, however, since all the missing beam momentum is assumed to be carried away by particles moving with the beam velocity and with zero transverse momenta.

BUU transport equations calculations, which do account for particle emission at non-zero emission angles, predict residue temperatures of about 3 MeV for calculations of the similar $^{40}Ar + ^{124}Sn$ system, assuming a soft EOS at low density [45]. Further measurements are needed to determine whether such calculations can also reproduce the energy spectra or other observables in this reaction.

## ACKNOWLEDGMENTS

This work is supported by the National Science Foundation under Grant No. PHY-89-13815 and the Department of Energy under Grant No. DE.FG-0288ER.40404.A W.G.L. acknowledges the receipt of U.S. Presidential Young Investigator Award and N.C. acknowledges partial support by the FAPESP, Brazil. Another of us (C.S.) acknowledges the receipt of a fellowship of the Deutsche Forschungsgemeinschaft (Federal Republic of Germany).

# REFERENCES

* Present address: Nuclear Science Division, Lawrence Berkeley Laboratory, Berkely, CA 94720, USA

† Present address: Instituto de Física, Universidade de São Paulo, C. Postal 20516, CEP 01498, São Paulo, Brazil.

‡ Present address: National Lab. for High Energy Physics (KEK), Department of Physics, 1-1 Oho, Tsukuba, Ibaraki 305, Japan.

§ Present address: Department of Physics, Kyoto University, Kyoto 606, Japan.

** Present address: Dipartimento di Fisica dell'Universitá and INFN, Largo Enrico Fermi 2, 50125 Firenze, Italy.

†† Present address: Department of Chemistry, Indiana University Cyclotron Facility, Indiana University, Bloomington, Indiana 47405, USA

‡‡ Present address: Cyclotron Institute, Texas A&M University, College Station, Texas 77843, USA

§§ Present address: P-2 Division, Los Alamos National Laboratory Los Alamos, New Mexico 87545

[1] D. J. Morrissey, W. Benenson, E. Kashy, B. Sherrill, A. D. Panagiotou, R. A. Blue, R. M. Ronningen, J. van der Plicht, and H. Utsunomiya, Phys. Lett. B **148**, 423 (1984).

[2] D. J. Morrissey, W. Benenson, E. Kashy, C. Bloch, M. Lowe, R. A. Blue, R. M. Ronningen, B. Sherrill, H. Utsunomiya, and I. Kelson, Phys. Rev. C **32**, 877 (1985).

[3] D. J. Morrissey, C. Bloch, W. Benenson, E. Kashy, R. A. Blue, R. M. Ronningen, and R. Aryaeinejad, Phys. Rev. C **34**, 761 (1986).

[4] H. M. Xu, D. J. Fields, W. G. Lynch, M. B. Tsang, C. K. Gelbke, M. Maier, D. J. Morrissey, J. Pochodzalla, D. G. Sarantites, L. G. Sobotka, M. L. Halbert, D. C. Hensley,

D. Hahn, and H. Stöcker, Phys. Lett. B **182**, 155 (1986).

[5] H. M. Xu, W. G. Lynch, C. K. Gelbke, M. B. Tsang, D. J. Fields, M. R. Maier, D. J. Morrissey, T. K. Nayak, J. Pochodzalla, D. G. Sarantites, L. G. Sobotka, M. L. Halbert, and D. C. Hensley, Phys. Rev. C **40**, 186 (1989).

[6] J. G. del Campo, J. L. Charvet, A. D'Onofrio, R. L. Auble, J. R. Beene, M. L. Halbert, and H. J. Kim, Phys. Rev. Lett. **61**, 290 (1988).

[7] J. G. del Campo, R. L. Auble, J. R. Beene, M. L. Halbert, H. J. Kim, A. D'Onofrio, and J. L. Charvet, Phys. Rev. C **43**, 2689 (1991).

[8] J. Pochodzalla, W. A. Friedman, C. K. Gelbke, W. G. Lynch, M. Maier, D. Ardouin, H. Delagrange, H. Doubre, C. Grégoire, A. Kyanowski, W. Mittig, A. Péghaire, J. Péter, F. Saint-Laurent, Y. P. Viyogi, B. Zwieglinski, G. Bizard, F. Lefébvres, B. Tamain, and J. Québert, Phys. Lett. B **161**, 275 (1985).

[9] J. Pochodzalla, W. A. Friedman, C. K. Gelbke, W. G. Lynch, M. Maier, D. Ardouin, H. Delagrange, H. Doubre, C. Grégoire, A. Kyanowski, W. Mittig, A. Péghaire, J. Péter, F. Saint-Laurent, Y. P. Viyogi, B. Zwieglinski, G. Bizard, F. Lefébvres, B. Tamain, and J. Québert, Phys. Rev. Lett. **55**, 177 (1985).

[10] J. Pochodzalla, C. K. Gelbke, W. G. Lynch, M. Maier, D. Ardouin, H. Delagrange, H. Doubre, C. Grégoire, A. Kyanowski, W. Mittig, A. Péghaire, J. Péter, F. Saint-Laurent, B. Zwieglinski, G. Bizard, F. Lefébvres, B. Tamain, J. Québert, Y. P. Viyogi, W. A. Friedman, and D. H. Boal, Phys. Rev. C **35**, 1695 (1987).

[11] Z. Chen, C. K. Gelbke, J. Pochodzalla, C. B. Chitwoood, D. J. Fields, W. G. Lynch, and M. B. Tsang, Phys. Lett. B **186**, 280 (1987).

[12] Z. Chen, C. K. Gelbke, J. Pochodzalla, C. B. Chitwoood, D. J. Fields, W. G. Gong, W. G. Lynch, and M. B. Tsang, Nucl. Phys. **A473**, 564 (1987).

[13] Z. Chen, C. K. Gelbke, W. G. Gong, Y. D. Kim, W. G. Lynch, M. R. Maier, J. Pochodzalla, M. B. Tsang, F. Saint-Laurent, D. Ardouin, H. Delagrange, H. Doubre, J. Kasagi, A. Kyanowski, A. Péghaire, J. Péter, E. Rosato, G. Bizard, F. Lefébvres, B. Tamain, J. Québert, and Y. P. Viyogi, Phys. Rev. C **36**, 2297 (1987).

[14] Z. Chen, C. K. Gelbke, W. G. Gong, Y. D. Kim, W. G. Lynch, M. R. Maier, J. Pochodzalla, M. B. Tsang, F. Saint-Laurent, D. Ardouin, H. Delagrange, H. Doubre, J. Kasagi, A. Kyanowski, A. Péghaire, J. Péter, E. Rosato, G. Bizard, F. Lefébvres, B. Tamain, J. Québert, and Y. P. Viyogi, Phys. Lett. B **199**, 171 (1987).

[15] F. Saint-Laurent, A. Kyanowski, , D. Ardouin, H. Delagrange, H. Doubre, C. Grégoire, W. Mittig, A. Péghaire, J. Péter, G. Bizard, F. Lefébvres, B.Tamain, J. Québert, Y. P. Viyogi, J. Pochodzalla, C. K. Gelbke, W. G. Lynch, and M. Maier, Phys. Lett. B **202**, 190 (1988).

[16] D. Fox, A. Cebra, J. Karn, C. Parks, A. Pradhan, A. /mboxVander Molen, J. van der Plicht, G. D. Westfall, W. K. Wilson, and R. S. Tickle, Phys. Rev. C **38**, 146 (1988).

[17] T. K. Nayak, T. Murakami, W. G. Lynch, K. Swartz, D. J. Fields, C. K. Gelbke, Y. D. Kim, J. Pochodzalla, M. B. Tsang, H. M. Xu, F. Zhu, and K. Kwiatkowski, Phys. Rev. Lett. **62**, 1021 (1989).

[18] T. K. Nayak, T. Murakami, W. G. Lynch, K. Swartz, D. J. Fields, C. K. Gelbke, Y. D. Kim, J. Pochodzalla, M. B. Tsang, H. M. Xu, F. Zhu, and K. Kwiatkowski, Phys. Rev. C **45**, 132 (1992).

[19] F. Zhu, W. G. Lynch, D. R. Bowman, R. T. de Souza, C. K. Gelbke, Y. D. Kim, L. Phair, M. B. Tsang, C. Williams, H. M. Xu, and J. Dinius, Phys. Lett. B **282**, 299 (1992).

[20] G. J. Kunde, J. Pochodzalla, J. Aichelin, E. Berdermann, B. Berthier, C. Cerruti, C. K. Gelbke, J. Hubele, P. Kreutz, S. Leray, R. Lucas, U. Lynen, U. Milkau, W. F. J. Müller,

C. Ngô, C. H. Pinkenburg, G. Raciti, H. Sann, and W. Trautmann, Phys. Lett. B **272**, 202 (1991).

[21] C. Bloch, W. Benenson, E. Kashy, D. J. Morrissey, R. A. Blue, R. Ronningen, and H. Utsunomiya, Phys. Rev. C **34**, 850 (1986).

[22] C. Bloch, W. Benenson, A. I. Galonsky, E. Kashy, J. Heltsley, L. Heilbronn, M. Lowe, B. Remington, D. J. Morrissey, and J. Kasagi, Phys. Rev. C **36**, 203 (1987).

[23] A. Galonsky, G. Caskey, L. Heilbronn, B. A. Remington, H. Schelin, F. Deák, A. Kiss, Z. Seres, and J. Kasagi, Phys. Lett. B **197**, 511 (1987).

[24] F. Deák, A. Kiss, Z. Seres, A. Galonsky, C. K. Gelbke, L. Heilbronn, W. G. Lynch, T. Murakami, H. Schelin, M. B. Tsang, B. A. Remington, and J. Kasagi, Phys. Rev. C **39**, 733 (1989).

[25] L. Heilbronn, A. Galonsky, C. K. Gelbke, W. G. Lynch, T. Murakami, D. Sackett, H. Schelin, M. B. Tsang, F. Deák, A. Kiss, Z. Seres, J. Kasagi, and B. A. Remington, Phys. Rev. C **43**, 2318 (1991).

[26] C. B. Chitwood, C. K. Gelbke, J. Pochodzalla, , Z. Chen, D. J. Fields, W. G. Lynch, R. Morse, M. B. Tsang, D. H. Boal, and J. C. Shillcock, Phys. Lett. B **172**, 27 (1986).

[27] H. Xi, W. Zhan, Y. Zhu, Z. Guo, X. Hu, G. Liu, J. Zhou, S. Yin, Y. Zhao, Z. Wei, and E. Fan, Nuc. Phys. **A552**, 281 (1993).

[28] J. Galin, Nuc. Phys. **A488**, 297c (1988).

[29] D. Jacquet, J. Galin, B. Borderie, D. Gardès, D. Guerreau, M. Lefort, F. Monnet, X. Tarrago, E. Duek, and J. M. Alexander, Phys. Rev. C **32**, 1594 (1985).

[30] J. B. Natowitz, M. Gonin, K. Hagel, R. Wada, S. Shlomo, X. Bin, M. Gui, Y. Lou, D. Utley, T. Botting, R. K. Choudhury, L. Cooke, B. Hurst, D. O'Kelly, R. P. Schmitt, W. Turmel, H. Utsunomiya, G. Nebbia, D. Fabris, J. A. Ruiz, G. Nardelli, M. Poggi,

R. Zanon, G. Viesti, R. H. Burch, F. Gramegna, G. Prete, D. Drain, B. Chambon, B. Cheynis, D. Guinet, X. Hu, A. Demeyer, C. Pastor, A. Giorni, A. Lleres, P. Stassi, B. Viano, A. M. Rocha, M. E. Brandan, and P. Gonthier, Nucl. Phys. **A538**, 263c (1992).

[31] D. Fabris, K. Hagel, J. B. Natowitz, G. Nebbia, R. Wada, R. Billery, B. Cheynis, A. Demeyer, D. Drain, D. Guinet, C. Pastor, L. Vagneron, K. Zaid, J. Alarja, A. Giorni, D. Heuer, C. Morand, B. Viano, C. Mazur, C. Ngô, S. Leray, R. Lucas, M. Ribrag, and E. Tomasi, Nucl. Phys. **A471**, 351c (1987).

[32] D. Fabris, K. Hagel, J. B. Natowitz, G. Nebbia, R. Wada, R. Billery, B. Cheynis, A. Demeyer, D. Drain, D. Guinet, C. Pastor, L. Vagneron, K. Zaid, J. Alarja, A. Giorni, D. Heuer, C. Morand, B. Viano, C. Mazur, C. Ngô, S. Leray, R. Lucas, M. Ribrag, and E. Tomasi, Phys. Lett. B **196**, 429 (1987).

[33] M. Gonin, J. P. Coffin, G. Guillaume, F. Jundt, P. Wagner, P. Fintz, B. Heusch, A. Malki, A. Fahli, S. Knox, F. Merchez, and J. Mistretta, Phys. Rev. C **38**, 135 (1988).

[34] K. Hagel, D. Fabris, P. Gonthier, H. Ho, Y. Lou, Z. Majka, G. Mouchaty, M. N. Namboodiri, J. B. Natowitz, G. Nebbia, R. P. Schmitt, G. Viesti, R. Wada, and B. Wilkins, Nuc. Phys. **A486**, 429 (1988).

[35] M. Gonin, L. Cooke, K. Hagel, Y. Lou, J. B. Natowitz, R. P. Schmitt, B. Srivastava, W. Turmel, H. Utsunomiya, R. Wada, B. Fornal, G. Nardelli, G. Nebbia, G. Viesti, R. Zanon, G. Prete, P. Gonthier, and B. Wilkins, Phys. Lett. B **217**, 406 (1989).

[36] M. Gonin, L. Cooke, K. Hagel, Y. Lou, J. B. Natowitz, R. P. Schmitt, S. Shlomo, B. Srivastava, W. Turmel, H. Utsunomiya, R. Wada, G. Nardelli, G. Nebbia, G. Viesti, R. Zanon, B. Fornal, G. Prete, K. Niita, S. Hannuschke, P. Gonthier, and B. Wilkins, Phys. Rev. C **42**, 2125 (1990).

[37] S. Song, M. F. Rivet, R. Bimbot, B. Borderie, I. Forest, J. Galin, D. Gardès, B. Gatty, M. Lefort, H. Oeschler, B. Tamain, and X. Tarrago, Phys. Lett. B **130**, 14 (1983).

[38] D. Hilscher, H. Rossner, A. Gamp, U. Jahnke, B. Cheynis, B. Chambon, D. Drain, C. Pastor, G. Giorni, C. Morand, A. Dauchy, P. Stassi, and G. Petitt, Phys. Rev. C **36**, 208 (1987).

[39] R. Wada, D. Fabris, K. Hagel, G. Nebbia, Y. Lou, M. Gonin, J. B. Natowitz, R. Billery, B. Cheynis, A. Demeyer, D. Drain, D. Guinet, C. Pastor, J. Alarja, A. Giorni, D. Heuer, C. Morand, B. Viano, C. Mazur, C. Ngô, S. Leray, R. Lucas, M. Ribrag, and E. Tomasi, Phys. Rev. C **39**, 497 (1989).

[40] D. X. Jiang, H. Doubre, J. Galin, D. Guerreau, E. Piasecki, J. Pouthas, A. Sokolov, B. Cramer, G. Ingold, U. Jahnke, E. Schwinn, J. L. Charvet, J. Frehaut, B. Lott, C. Magnago, M. Morjean, Y. Patin, Y. Pranal, J. L. Uzureau, B. Gatty, and D.Jacquet, Nuc. Phys. **A503**, 560 (1989).

[41] W. Bohne, H. Morgenstern, K. Grabisch, T. Nakagawa, and S. Proschitzki, Phys. Rev. C **41**, R5 (1990).

[42] A. Chbihi, L. G. Sobotka, N. G. Nicolis, D. G. Sarantites, D. W. Stracener, Z. Majka, D. C. Hensley, J. R. Beene, and M. L. Halbert, Phys. Rev. C **43**, 666 (1991).

[43] H. W. Barz, J. P. Bondorf, and H. Schulz, Phys. Lett. B **184**, 125 (1987).

[44] W. A. Friedman, Phys. Rev. Lett. **60**, 2125 (1988).

[45] H. M. Xu, P. Danielewicz, and W. G. Lynch, Phys. Lett. B **299**, 199 (1992).

[46] D. H. Boal, N. Glosli, and C. Wicentowich, Phys. Rev. Lett. **62**, 737 (1989).

[47] J. Bondorf, R. Donangelo, I. N. Mishustin, and H. Schulz, Nucl. Phys. **A444**, 460 (1985).

[48] D. H. E. Gross and H. Massmann, Nucl. Phys. **A471**, 339c (1987).

[49] H. Fuchs and H. Homeyer, in *Proceedings of the International Workshop on Particle Correlations and Interferometry in Nuclear Collisions*, edited by D. Ardouin (World Scientific, Singapore, 1990, held at Nantes, 1990), p. 305.

[50] S. Ban-Hao and D. H. E. Gross, Nucl. Phys. **A437**, 643 (1985).

[51] P. J. Siemens and J. O. Rasmussen, Phys. Rev. Lett. **42**, 880 (1979).

[52] M. B. Tsang, C. B. Chitwood, D. J. Fields, C. K. Gelbke, D. R. Klesch, W. G. Lynch, K. Kwiatkowski, and V. E. Viola Jr, Phys. Rev. Lett. **52**, 1967 (1984).

[53] M. B. Tsang, R. M. Ronningen, G. Bertsch, Z. Chen, C. B. Chitwood, D. J. Fields, C. K. Gelbke, W. G. Lynch, T. Nayak, J. Pochodzalla, T. Shea, and W. Trautmann, Phys. Rev. Lett. **57**, 559 (1986).

[54] M. B. Tsang, W. G. Lynch, R. M. Ronningen, Z. Chen, C. K. Gelbke, T. Nayak, J. Pochodzalla, F. Zhu, M. Tohyama, W. Trautmann, and W. Dünnweber, Phys. Rev. Lett. **60**, 1479 (1988).

[55] W. Terlau, M. Bürgel, A. Budzanowski, H. Fuchs, H. Homeyer, G. Röschert, J. Uckert, and R. Vogel, Z. Phys. A **330**, 303 (1988).

[56] C. Schwarz, H. Fuchs, H. Homeyer, K. Möhring, T. Schmidt, A. Siwek, A. Sourell, W. Terlau, and A. Budzanowski, Phys. Lett. B **279**, 223 (1992).

[57] K. Möhring, T. Srokowski, D. H. E. Gross, and H. Homeyer, Phys. Lett. B **203**, 210 (1988).

[58] K. Möhring, T. Srokowski, and D. H. E. Gross, Nucl. Phys. **A533**, 333 (1991).

[59] W. A. Friedman and W. G. Lynch, Phys. Rev. C **28**, 16 (1983).

[60] D. J. Fields, W. G. Lynch, C. B. Chitwood, C. K. Gelbke, M. B. Tsang, H. Utsunomiya, and J. Aichelin, Phys. Rev. C **30**, 1912 (1984).

[61] Z. Chen and C. K. Gelbke, Phys. Rev. C **38**, 2630 (1988).

[62] W. G. Gong, Y. D. Kim, G. Poggi, Z. Chen, C. K. Gelbke, W. G. Lynch, M. R. Maier, T. Murakami, M. B. Tsang, and H. M. Xu, Nucl. Instrum. and Meth. **A268**, 190 (1988).

[63] W. G. Gong, Ph.D. thesis, Michigan State University, 1991.

[64] D. J. Fields, W. G. Lynch, T. K. Nayak, M. B. Tsang, C. B. Chitwood, C. K. Gelbke, R. Morse, J. Wilczynski, T. C. Awes, R. L. Ferguson, F. Plasil, F. E. Obenshain, and G. R. Young, Phys. Rev. C **34**, 536 (1986).

[65] W. G. Gong, C. K. Gelbke, W. Bauer, N. Carlin, R. T. de Souza, Y. D. Kim, W. G. Lynch, T. Murakami, G. Poggi, D. P. Sanderson, M. B. Tsang, H. M. Xu, D. J. Fields, K. Kwiatkowski, R. Planeta, V. E. Viola, S. J. Yennello, and S. Pratt, Phys. Rev. C **43**, 1804 (1991).

[66] A. M. Lane and R. G. Thomas, Rev. Mod. Phys. **30**, 257 (1958).

[67] I. Y. Barit and V. A. Sergeev, Sov. J. Nucl. Phys. **13**, 708 (1971).

[68] T. Stammbach and R. L. Walter, Nucl. Phys. **A180**, 225 (1972).

[69] W. E. Kunz, Phys. Rev. **97**, 456 (1955).

[70] F. C. Barker and P. B. Treacy, Nucl. Phys. **38**, 33 (1962).

[71] J. Pochodzalla, W. A. Friedman, C. K. Gelbke, W. G. Lynch, M. Maier, D. Ardouin, H. Delagrange, H. Doubre, C. Grégoire, A. Kyanowski, W. Mittig, A. Péghaire, J. Péter, F. Saint-Laurent, Y. P. Viyogi, B. Zwieglinski, G. Bizard, F. Lefébvres, B. Tamain, and J. Québert, Phys. Lett. B **161**, 256 (1985).

[72] F. Ajzenberg-Selove, Nucl. Phys. **A490**, 1 (1988).

[73] D. R. Tilley, H. R. Weller, and G. M. Hale, Nucl. Phys. **A541**, 1 (1992).

[74] P. E. Koehler, C. D. Bowman, F. J. Steinkruger, D. C. Moody, G. M. Hale, J. W. Starner, S. A. Wender, R. C. Haight, P. W. Lisowski, and W. L. Talbert, Phys. Rev. C **37**, 917 (1988).

[75] H. Dabrowski, D. Goujdami, F. Guilbault, C. Lebrun, D. Ardouin, P. Lautridou, R.

Boisgard, J. Québert, A. Péghaire, P. Eudes, F. Sébille, and B. Remaud, Phys. Lett. B **247**, 223 (1990).

[76] D. H. Boal and J. N. Glosli, Phys. Rev. C **37**, 91 (1988).

[77] D. H. Boal and J. N. Glosli, Phys. Rev. C **42**, R502 (1990).

[78] V. E. Viola, Nucl. Phys. **A471**, 53c (1987).

[79] M. Fatyga, K. Kwiatkowski, V. E. Viola, C. B. Chitwood, D. J. Fields, C. K. Gelbke, W. G. Lynch, J. Pochodzalla, M. B. Tsang, and M. Blann, Phys. Rev. Lett. **55**, 1376 (1985).

## TABLES

TABLE I. Fit parameters used for the description of the inclusive single fragment cross sections shown in Figs. 1, 2, 3. The spectra for the $^{14}$N- and $^{129}$Xe-induced reactions were fitted with Eqs. (1) and (2), respectively. The normalization constants $N_i$ are given in units of mb/(sr×MeV$^{3/2}$). Also given are the velocities $\beta_{pro}$ and $\beta_{CN}$ of the projectile and the compound nucleus.

| Reaction | Fragment | $\beta_{pro}$ | $\beta_{CN}$ | $U_C$ [MeV] | $\Delta_C$ [MeV] | $i$ | $N_i$ | $\beta_i$ | $T_i$ [MeV] |
|---|---|---|---|---|---|---|---|---|---|
| $^{14}$N+$^{27}$Al | $^{4}$He | 0.40 | 0.14 | 5.85 | | 1 | 0.59 | 0.340 | 7.9 |
| | | | | | | 2 | 0.11 | 0.233 | 14.1 |
| | | | | | | 3 | 0.25 | 0.104 | 9.1 |
| | $^{6}$Li | 0.40 | 0.14 | 8.01 | | 1 | $1.8 \times 10^{-2}$ | 0.330 | 10.7 |
| | | | | | | 2 | $5.3 \times 10^{-3}$ | 0.206 | 15.7 |
| | | | | | | 3 | $3.5 \times 10^{-2}$ | 0.084 | 8.3 |
| | $^{7}$Be | 0.40 | 0.14 | 9.93 | | 1 | $1.5 \times 10^{-2}$ | 0.331 | 11.1 |
| | | | | | | 2 | $3.8 \times 10^{-3}$ | 0.211 | 14.3 |
| | | | | | | 3 | 2.93 | 0.056 | 7.1 |
| $^{14}$N+$^{197}$Au | $^{4}$He | 0.40 | 0.026 | 17.9 | | 1 | 1.35 | 0.334 | 8.7 |
| | | | | | | 2 | 0.33 | 0.207 | 18.2 |
| | | | | | | 3 | 1.38 | 0.077 | 10.0 |
| | $^{6}$Li | 0.40 | 0.026 | 25.8 | | 1 | $7.0 \times 10^{-2}$ | 0.352 | 9.8 |
| | | | | | | 2 | $9.9 \times 10^{-3}$ | 0.235 | 21.0 |
| | | | | | | 3 | $2.9 \times 10^{-2}$ | 0.099 | 14.8 |
| | $^{7}$Be | 0.40 | 0.026 | 33.6 | | 1 | $2.3 \times 10^{-2}$ | 0.339 | 12.1 |
| | | | | | | 2 | $4.0 \times 10^{-3}$ | 0.209 | 20.0 |
| | | | | | | 3 | $7.9 \times 10^{-2}$ | 0.058 | 12.2 |
| $^{129}$Xe+$^{27}$Al | $^{4}$He | 0.26 | 0.21 | 13.1 | 3.5 | 1 | 157 | 0.228 | 4.4 |
| | | | | | | 2 | 32.6 | 0.039 | 25.3 |

| | | | | | | | | | |
|---|---|---|---|---|---|---|---|---|---|
| | $^{6}$Li | 0.26 | 0.21 | 21.5 | 7 | 1 | 1.34 | 0.220 | 6.6 |
| | | | | | | 2 | 2.02 | 0.003 | 28.5 |
| | $^{7}$Be | 0.26 | 0.21 | 24.5 | 6 | 1 | 0.27 | 0.210 | 10.0 |
| | | | | | | 2 | 4.23 | 0.004 | 16.6 |
| $^{129}$Xe+$^{122}$Sn | $^{4}$He | 0.26 | 0.13 | 7.8 | 7.5 | 1 | 210 | 0.211 | 6.2 |
| | | | | | | 2 | 42.8 | 0.048 | 22.9 |
| | $^{6}$Li | 0.26 | 0.13 | 15.0 | 11 | 1 | 2.28 | 0.194 | 11.2 |
| | | | | | | 2 | 2.33 | 0.014 | 17.2 |
| | $^{7}$Be | 0.26 | 0.13 | 19.6 | 15 | 1 | 0.54 | 0.189 | 12.8 |
| | | | | | | 2 | 28.1 | 0.019 | 9.9 |

TABLE II. The correlation functions for different two-particle combinations were normalized to unity at sufficient high relative momentum. The table shows the relative momentum range in MeV/c used for this normalization for different particle pairs and target-projectile combinations.

| particle pair | $^{14}$N+$^{197}$Au | $^{14}$N+$^{27}$Al | $^{129}$Xe+$^{27}$Al | $^{129}$Xe+$^{122}$Sn |
|---|---|---|---|---|
| p-t | 160-300 | 100-200 | 100-200 | 110-200 |
| p-$\alpha$ | 130-200 | 110-160 | 90-140 | 110-180 |
| d-$^{3}$He | 150-220 | 150-220 | 120-220 | 120-220 |
| $\alpha$-$\alpha$ | 260-330 | 260-330 | 260-330 | 260-330 |
| p-$^{7}$Li | 130-190 | 130-190 | 130-190 | 130-190 |

## FIGURES

FIG. 1. Inclusive $^{4}$He yields, measured at $\Theta_{lab}$ = $18^0$, $25^0$, and $33^0$, for the reactions $^{129}$Xe + $^{27}$Al and $^{129}$Xe + $^{122}$Sn at E/A=31 MeV (bottom panels) and the reactions $^{14}$N + $^{27}$Al and $^{14}$N + $^{197}$Au at E/A=75 MeV (top panels)

FIG. 2. Inclusive $^{6}$Li yields, measured at $\Theta_{lab}$ = $18^0$, $25^0$, and $33^0$, for the reactions $^{129}$Xe + $^{27}$Al and $^{129}$Xe + $^{122}$Sn at E/A=31 MeV (bottom panels) and the reactions $^{14}$N + $^{27}$Al and $^{14}$N + $^{197}$Au at E/A=75 MeV (top panels).

FIG. 3. Inclusive $^{7}$Be yields measured at $\Theta_{lab}$ = $18^0$, $25^0$, and $33^0$, for the reactions $^{129}$Xe + $^{27}$Al and $^{129}$Xe + $^{122}$Sn at E/A=31 MeV (bottom panels) and the reactions $^{14}$N + $^{27}$Al and $^{14}$N + $^{197}$Au at E/A=75 MeV (top panels).

FIG. 4. p-t correlation functions for the reaction systems $^{14}$N+$^{27}$Al and $^{14}$N+$^{197}$Au at E/A=75 MeV (upper panels), and $^{129}$Xe+$^{27}$Al and $^{129}$Xe+$^{122}$Sn at E/A=31 MeV (lower panels). The dashed lines are extreme bounds for the background correlation function. The solid line is a calculation with $T$ = 5 MeV for the $^{14}$N and $T$ = 3 MeV for the $^{129}$Xe-induced reactions for a background correlation function between the two extremes. For normalization see Tab. II.

FIG. 5. p-$\alpha$ correlation functions for different reaction systems. The dashed lines are extreme bounds for the background correlation function. The solid line is a calculation with $T$ = 4 MeV for the $^{14}$N and $T$ = 3 MeV for the $^{129}$Xe-induced reactions assuming the maximum background correlation function. The peak at $q \approx 15$ MeV/q corresponds to a three-body decay $^{9}B \rightarrow 2\alpha + p$ and not to a decay of an $A$ = 5 system. For normalization see Tab. II.

FIG. 6. d-$^{3}$He correlation functions for different reaction systems. The dashed lines are extreme bounds for the background correlation function. The solid line is a calculation with $T$ = 4 MeV for the $^{14}$N and $T$ = 3 MeV for the $^{129}$Xe-induced reactions assuming a background correlation function between the two extremes. For normalization see Tab. II.

FIG. 7. $\alpha-\alpha$ correlation functions for different reaction systems. The dashed lines are extreme bounds for the background correlation function. The solid line is a calculation with $T = 4$ MeV for the $^{14}$N and $T = 3$ MeV for the $^{129}$Xe-induced reactions assuming the minimum background correlation function. The peak at q=45 MeV/c is largely due to the decay of the 2.43 MeV state in $^{9}$Be ($^{9}Be \rightarrow 2\alpha + n$); in addition, it contains contributions from the "ghost peak" of the $^{8}$Be ground state (see Ref [10] and references therein). For normalization see Tab. II.

FIG. 8. p-$^{7}$Li correlation functions for different reaction systems. The dashed lines are extreme bounds for the background correlation function. The solid line is a calculation with $T = 4$ MeV for the $^{14}$N and $T = 3$ MeV for the $^{129}$Xe-induced reactions assuming the maximum background correlation function. For normalization see Tab. II.

FIG. 9. Ratios between the ($J^{\pi} = 0^{+}$) state at 20.21 MeV and the total yield of $^{4}$He. The upper panels show $^{14}$N+$^{27}$Al (left) and $^{14}$N+$^{197}$Au (right) at E/A=75 MeV, the lower panel $^{129}$Xe+$^{27}$Al (left) and $^{129}$Xe+$^{122}$Sn (right) at E/A=31 MeV, respectively.

FIG. 10. Ratios between the ($J^{\pi} = 3/2^{+}$) state at 16.7 MeV in $^{5}$Li and the ($J^{\pi} = 3/2^{-}$) particle-unstable "ground state". The upper panels show $^{14}$N+$^{27}$Al (left) and $^{14}$N+$^{197}$Au (right) at E/A=75 MeV, the lower panel $^{129}$Xe+$^{27}$Al (left) and $^{129}$Xe+$^{122}$Sn (right) at E/A=31 MeV, respectively.

FIG. 11. Ratios between the ($J^{\pi} = 1^{+}$) state in $^{8}$Be at 17.64 MeV and the ($J^{\pi} = 2^{+}$) state at 3.04 MeV. The upper panels show $^{14}$N+$^{27}$Al (left) and $^{14}$N+$^{197}$Au (right) at E/A=75 MeV, the lower panel $^{129}$Xe+$^{27}$Al (left) and $^{129}$Xe+$^{122}$Sn (right) at E/A=31 MeV, respectively.

FIG. 12. Extracted apparent temperatures from widely spaced levels of the fragments $^{4}$He, $^{5}$Li, and $^{8}$Be. The uncertainties are due to the extreme assumptions of the background correlation functions indicated in Figs. 4-8. The fragment averaged temperature bounds are marked by dashed lines. (For $^{129}$Xe-induced reactions the average was taken over the $^{4}$He and $^{8}$Be fragments.)

FIG. 13. Systematics of emission temperature parameters extracted for light projectiles impinging on heavy targets. The upper, medium, and lower panels show temperatures extracted from relative populations of unbound states for $^{4}$He, $^{5}$Li, and $^{8}$Be fragments, respectively. We included temperature parameters from [20] (crosses), [10,18,26] (open diamonds), [27] (star), and data ($^{14}$N+$^{197}$Au) from this work (solid diamonds). Additional temperatures from the reaction $^{129}$Xe+$^{27}$Al (this work) are plotted at E/A=31 MeV (solid circles). The dashed lines show a least square fit to the full set of data.

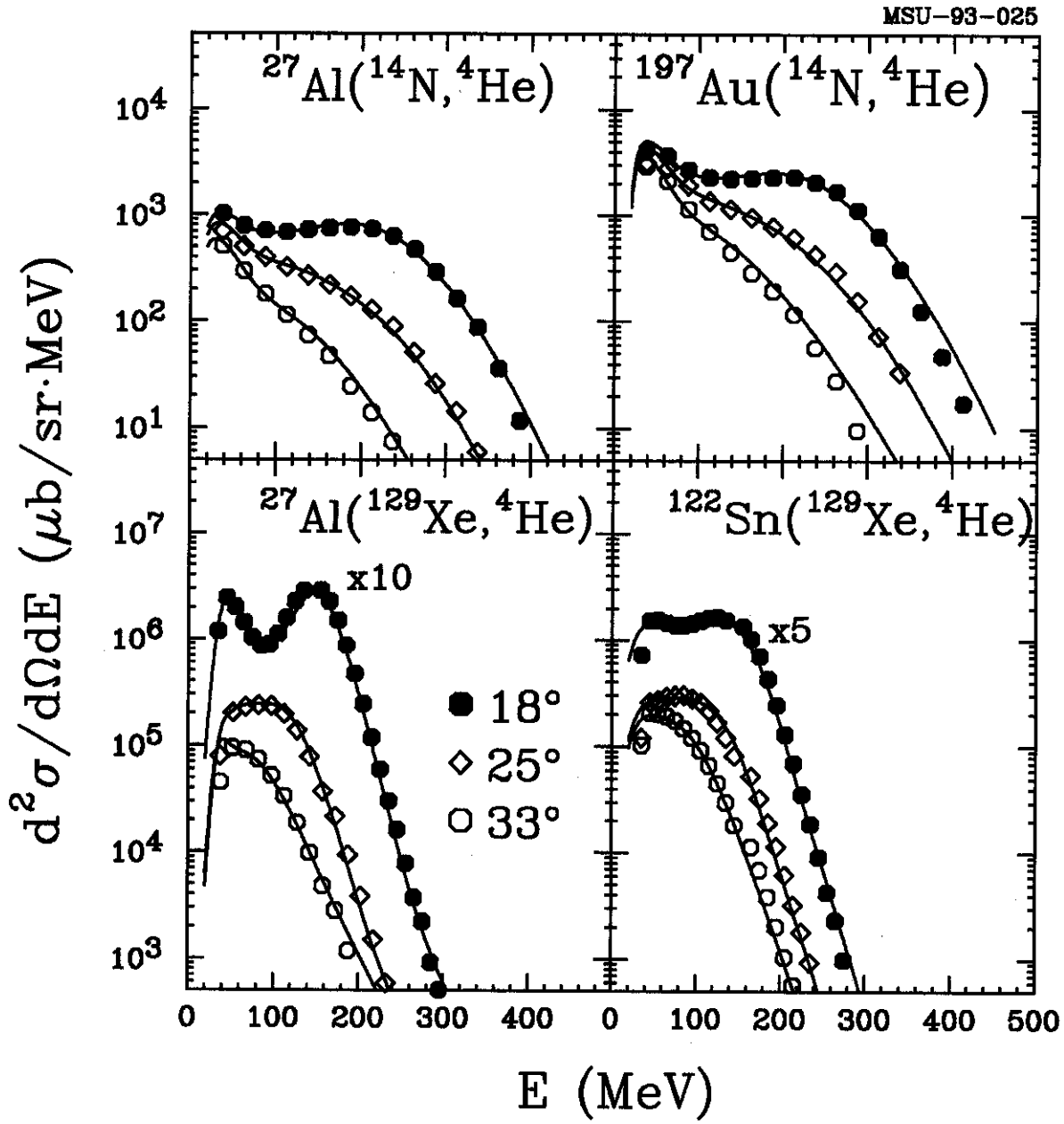
MSU-93-025
$^{27}$Al($^{14}$N,$^{4}$He)
$^{197}$Au($^{14}$N,$^{4}$He)
$^{27}$Al($^{129}$Xe,$^{4}$He)
$^{122}$Sn($^{129}$Xe,$^{4}$He)
x10
x5
18°
25°
33°
$d^2\sigma/d\Omega dE$ ($\mu$b/sr·MeV)
E (MeV)

Fig. 1

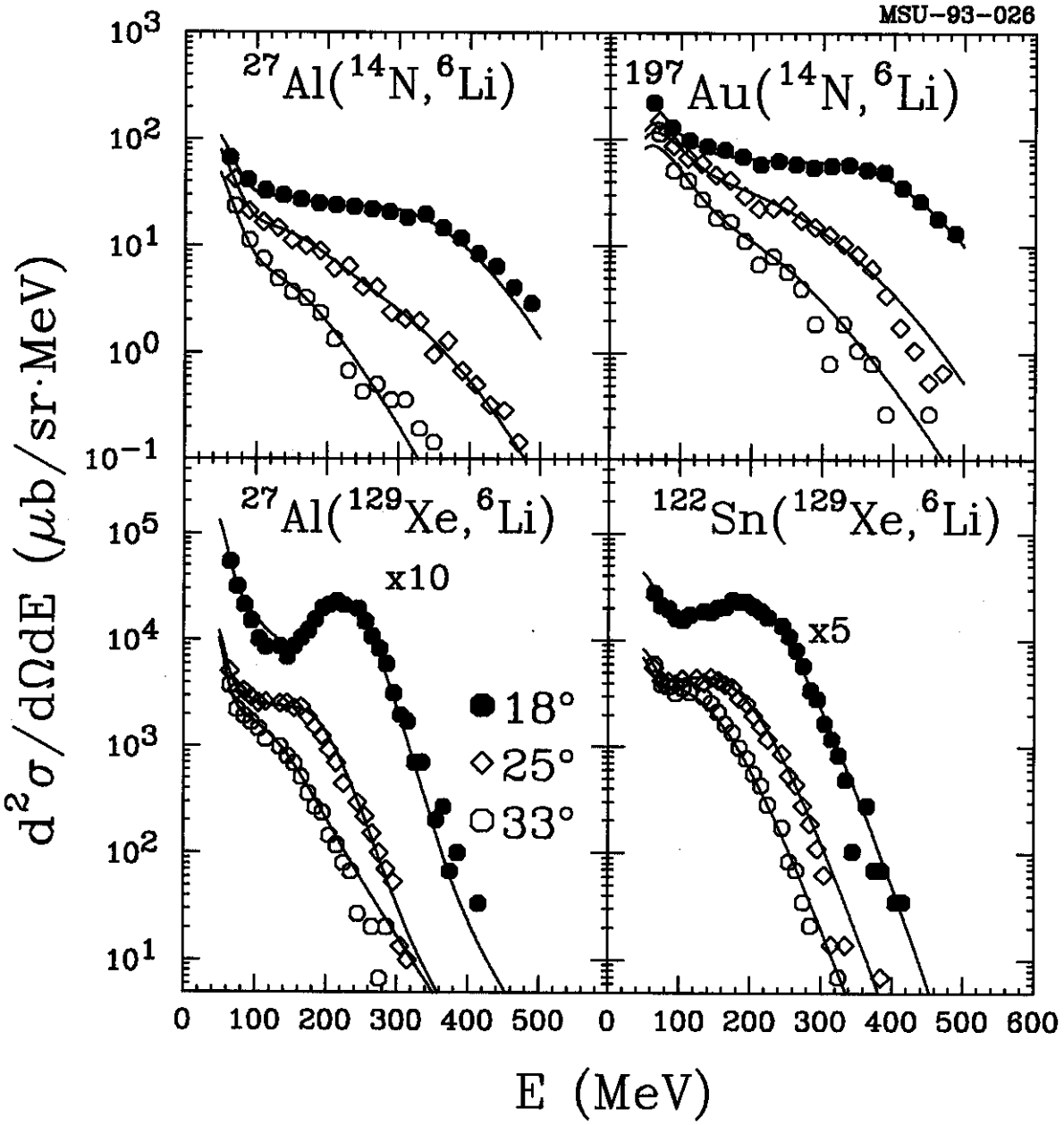
MSU-93-026
$^{27}$Al($^{14}$N,$^{6}$Li)
$^{197}$Au($^{14}$N,$^{6}$Li)
$^{27}$Al($^{129}$Xe,$^{6}$Li)
$^{122}$Sn($^{129}$Xe,$^{6}$Li)
x10
x5
18°
25°
33°
$d^2\sigma/d\Omega dE$ ($\mu$b/sr·MeV)
E (MeV)

Fig. 2

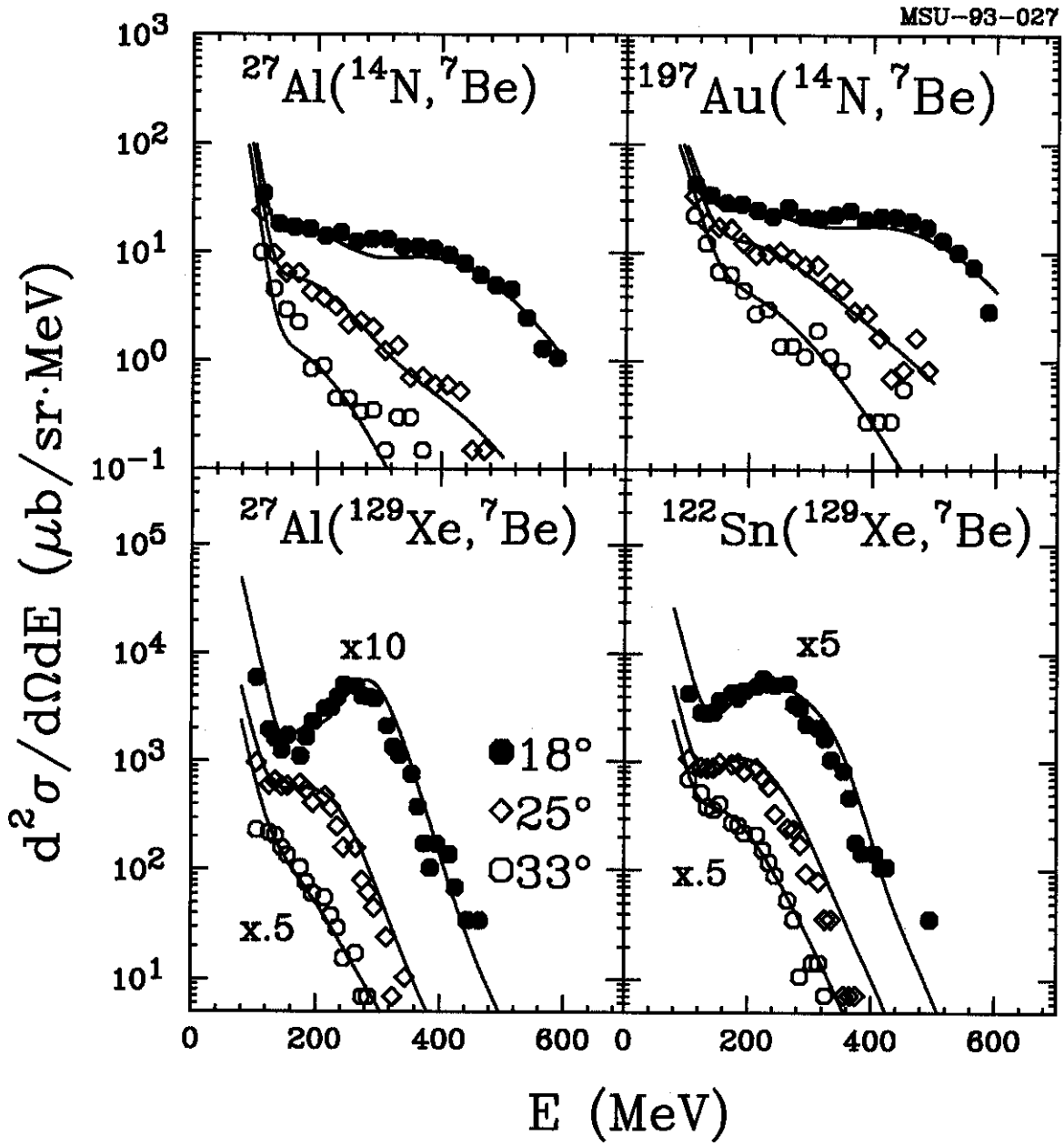
MSU-93-027
$^{27}$Al($^{14}$N,$^{7}$Be)
$^{197}$Au($^{14}$N,$^{7}$Be)
$^{27}$Al($^{129}$Xe,$^{7}$Be)
$^{122}$Sn($^{129}$Xe,$^{7}$Be)
x10
x.5
x5
x.5
18°
25°
33°
$d^2\sigma/d\Omega dE$ ($\mu$b/sr·MeV)
E (MeV)

Fig. 3

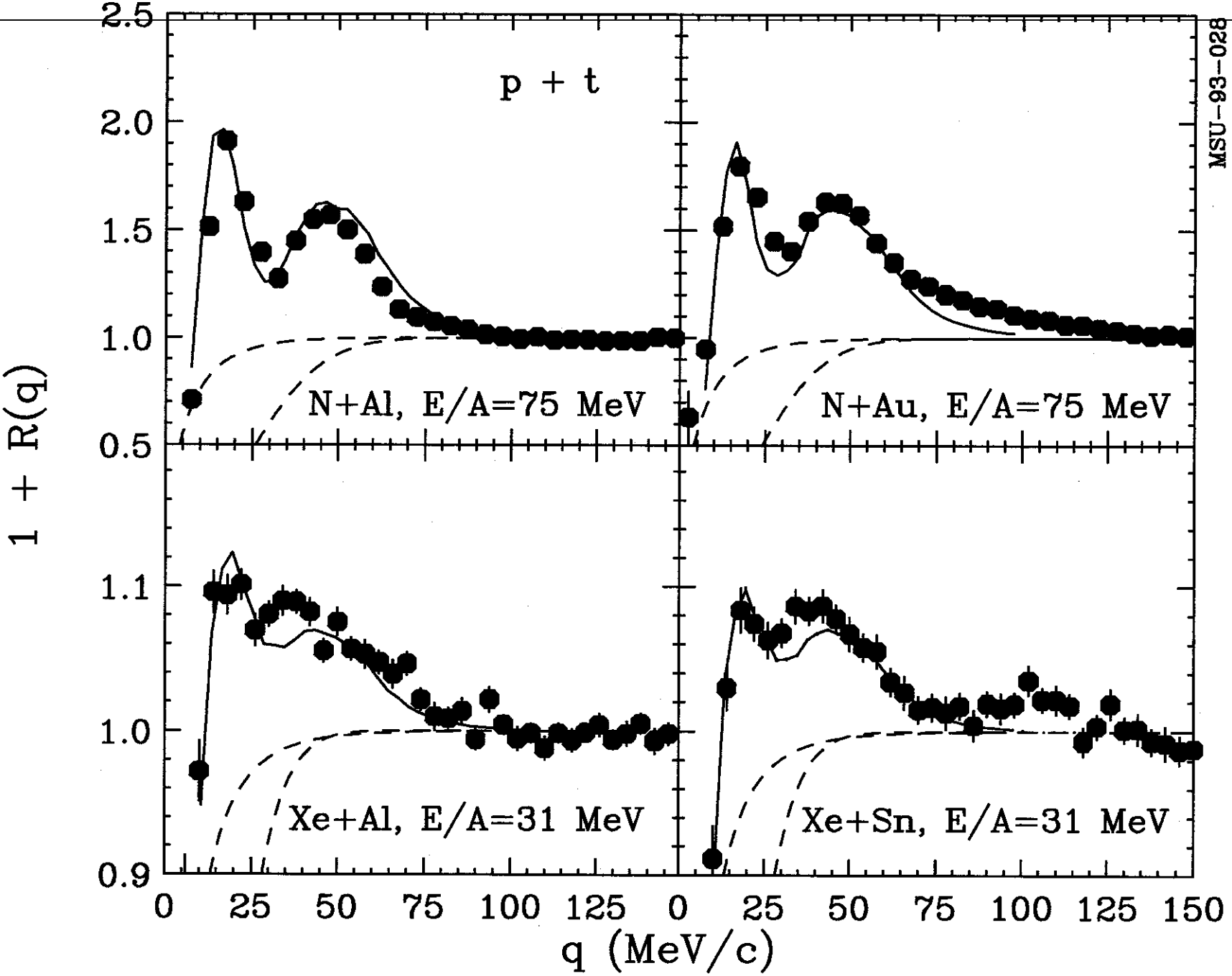
p + t
N+Al, E/A=75 MeV
N+Au, E/A=75 MeV
Xe+Al, E/A=31 MeV
Xe+Sn, E/A=31 MeV
1 + R(q)
q (MeV/c)
MSU-93-028
2.5
2.0
1.5
1.0
0.5
1.1
1.0
0.9
0
25
50
75
100
125
150

Fig. 4

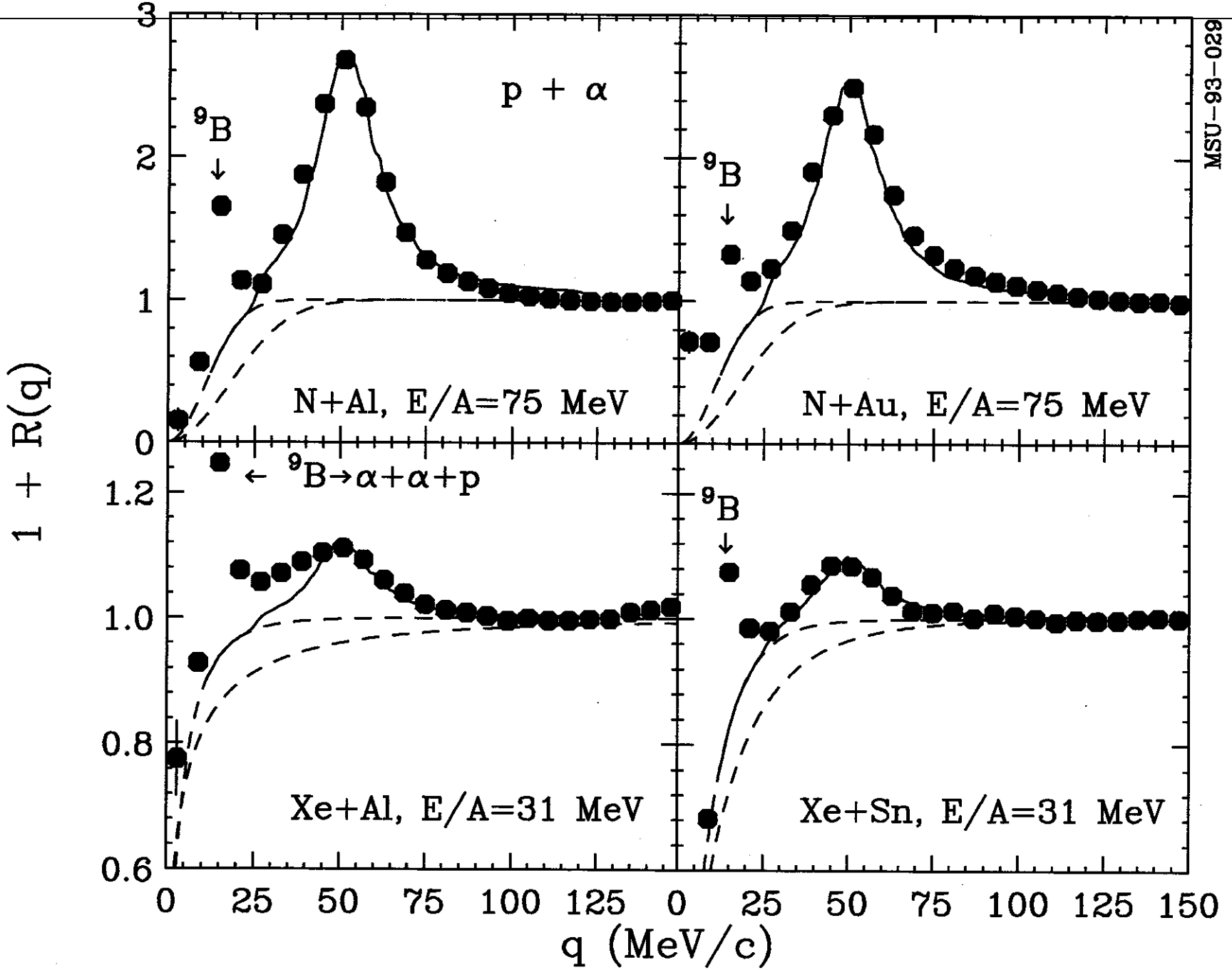
p + α
$^9$B
N+Al, E/A=75 MeV
N+Au, E/A=75 MeV
← $^9$B→α+α+p
Xe+Al, E/A=31 MeV
Xe+Sn, E/A=31 MeV
1 + R(q)
q (MeV/c)
MSU−93−029

Fig. 5

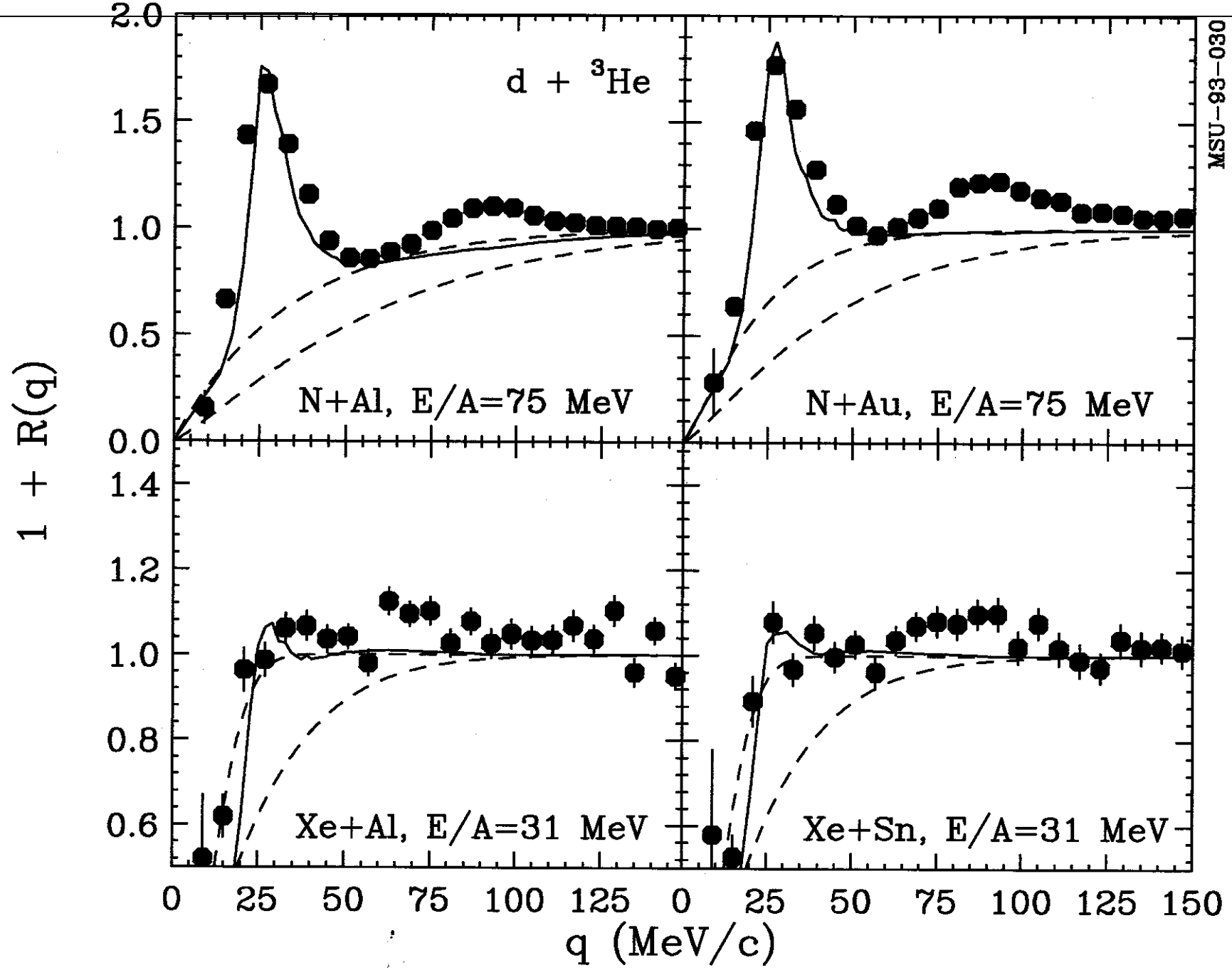
d + ³He
N+Al, E/A=75 MeV
N+Au, E/A=75 MeV
Xe+Al, E/A=31 MeV
Xe+Sn, E/A=31 MeV
1 + R(q)
q (MeV/c)
MSU−93−030

Fig. 6

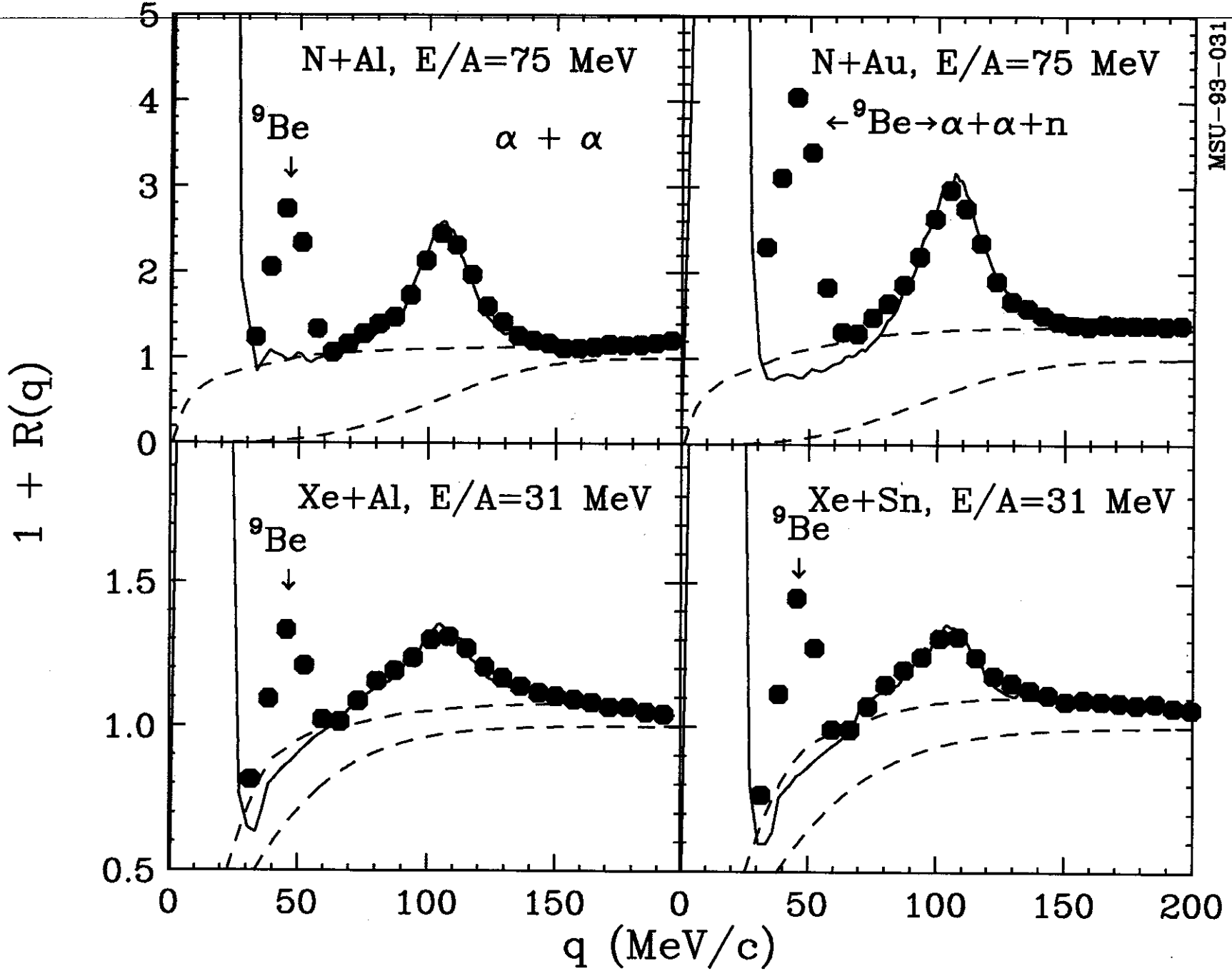
N+Al, E/A=75 MeV
$^9$Be
α + α
N+Au, E/A=75 MeV
←$^9$Be→α+α+n
Xe+Al, E/A=31 MeV
$^9$Be
Xe+Sn, E/A=31 MeV
$^9$Be
1 + R(q)
q (MeV/c)
MSU-93-031

Fig. 7

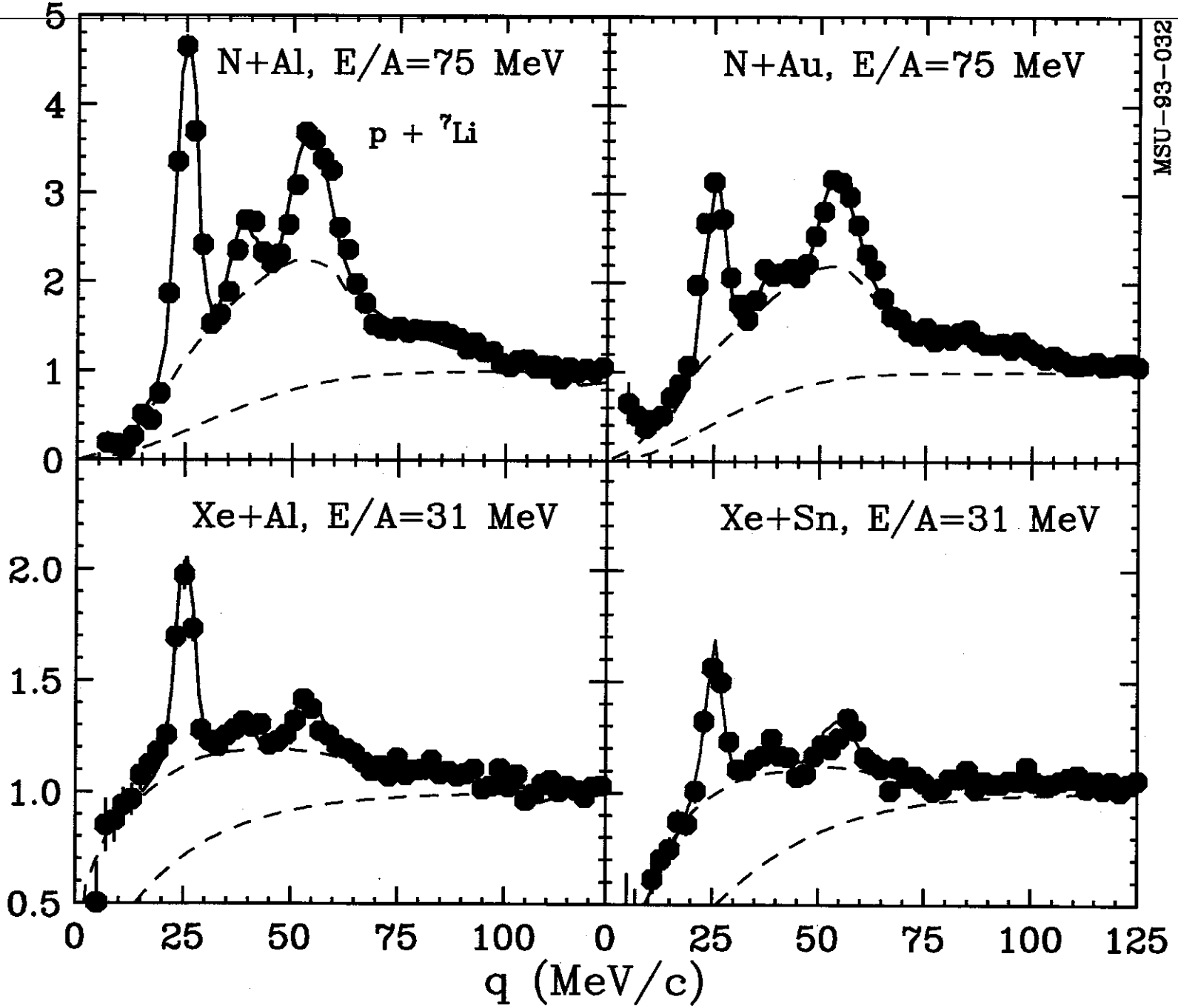
N+Al, E/A=75 MeV
p + $^7$Li
N+Au, E/A=75 MeV
Xe+Al, E/A=31 MeV
Xe+Sn, E/A=31 MeV
1 + R(q)
q (MeV/c)
MSU-93-032

Fig. 8

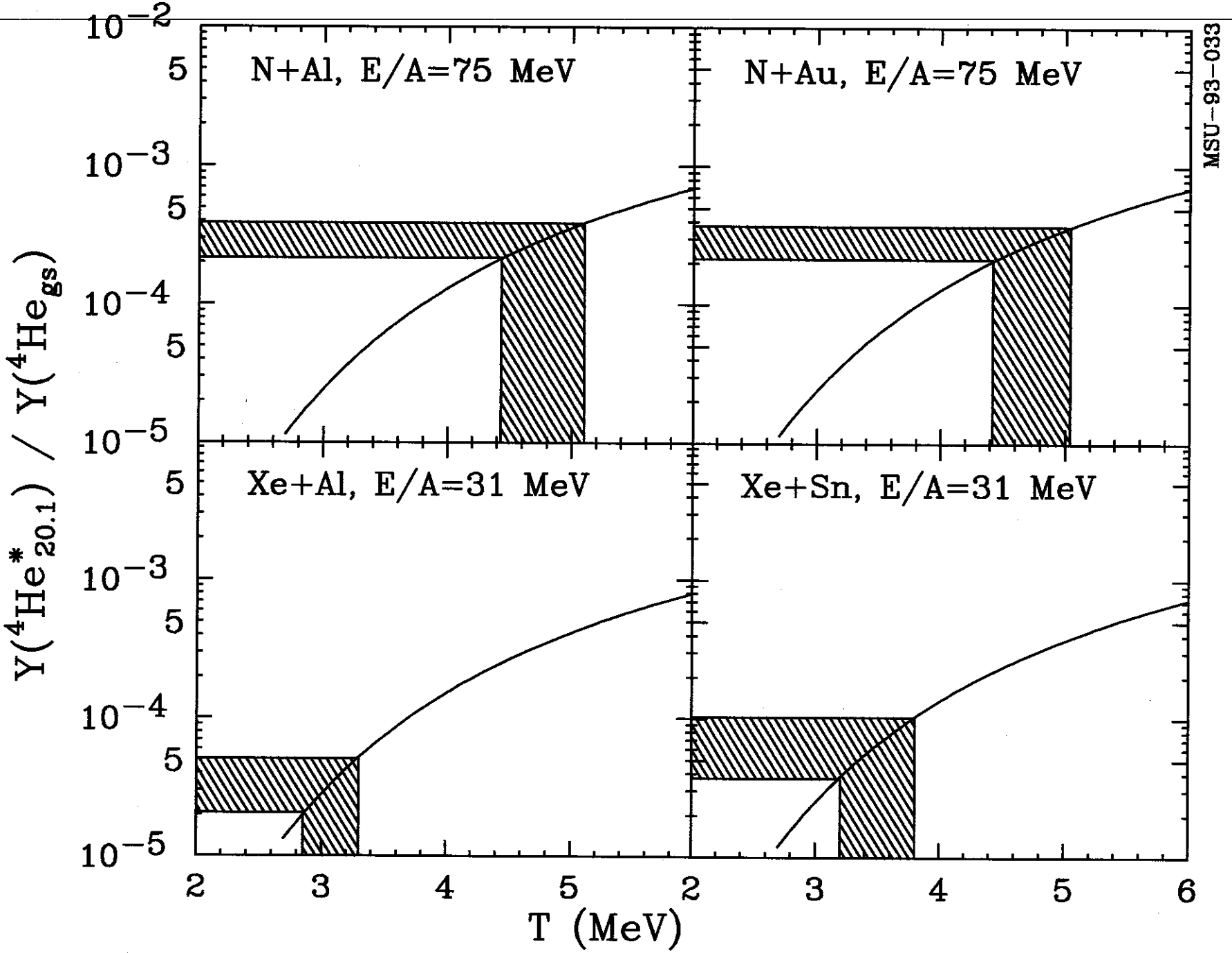
N+Al, E/A=75 MeV
N+Au, E/A=75 MeV
Xe+Al, E/A=31 MeV
Xe+Sn, E/A=31 MeV
MSU−93−033
Y(4He*20.1) / Y(4Hegs)
T (MeV)
10−2
10−3
10−4
10−5
5
2
3
4
5
6

Fig. 9

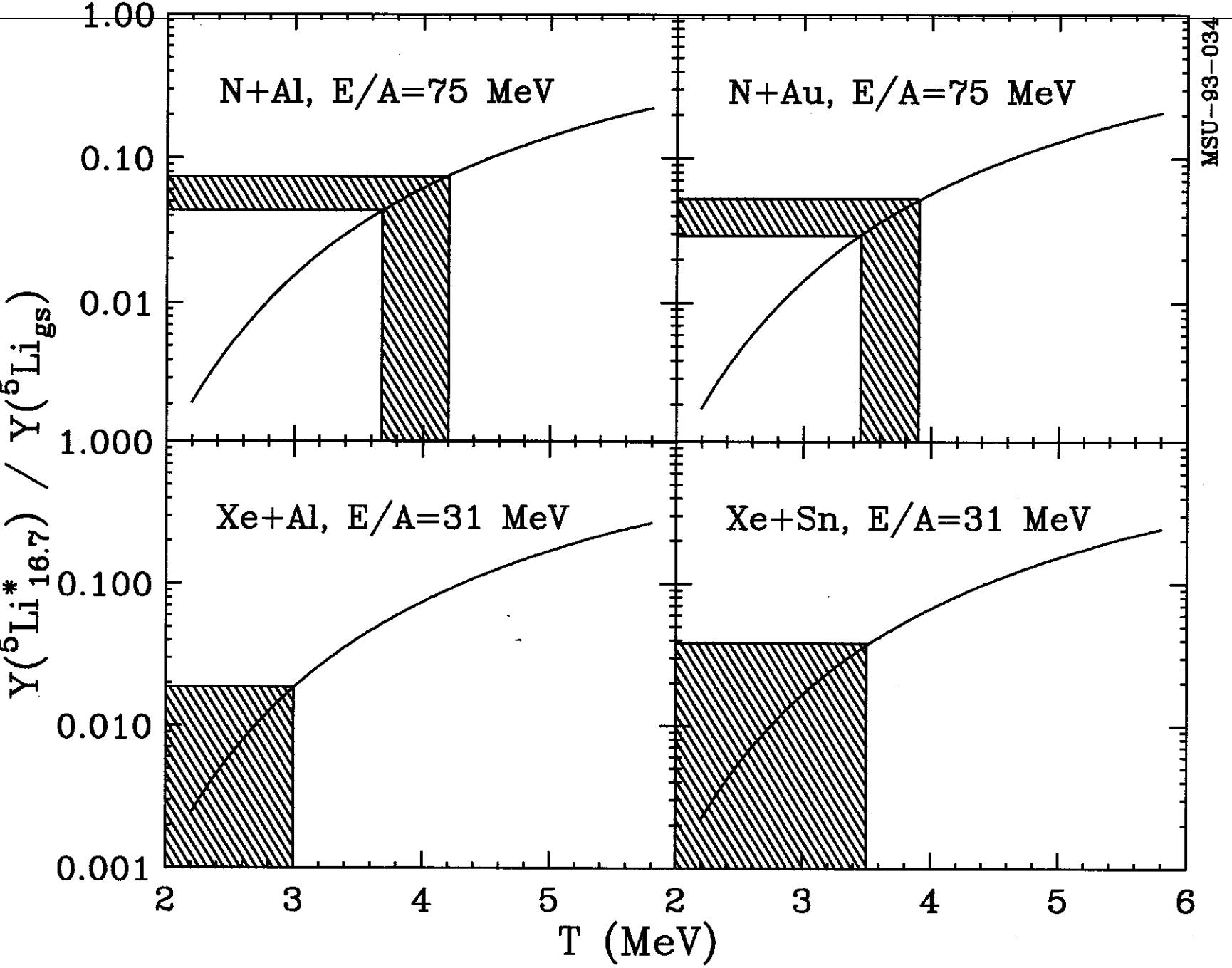
N+Al, E/A=75 MeV
N+Au, E/A=75 MeV
Xe+Al, E/A=31 MeV
Xe+Sn, E/A=31 MeV
MSU-93-034
1.00
0.10
0.01
1.000
0.100
0.010
0.001
2
3
4
5
6
T (MeV)
Y(5Li*16.7) / Y(5Ligs)

Fig. 10

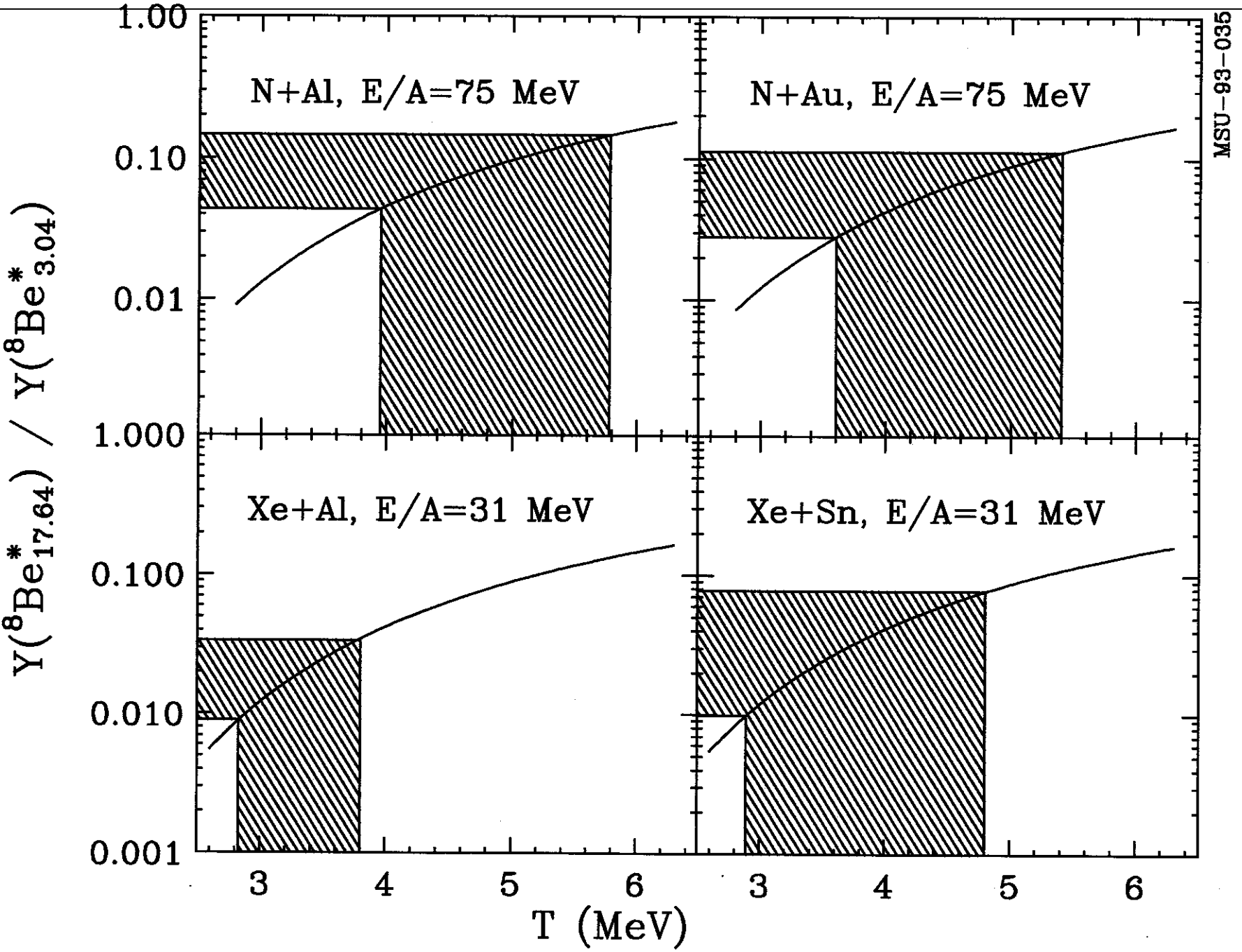
N+Al, E/A=75 MeV
N+Au, E/A=75 MeV
Xe+Al, E/A=31 MeV
Xe+Sn, E/A=31 MeV
1.00
0.10
0.01
1.000
0.100
0.010
0.001
3
4
5
6
T (MeV)
Y(8Be*17.64) / Y(8Be*3.04)
MSU-93-035

Fig. 11

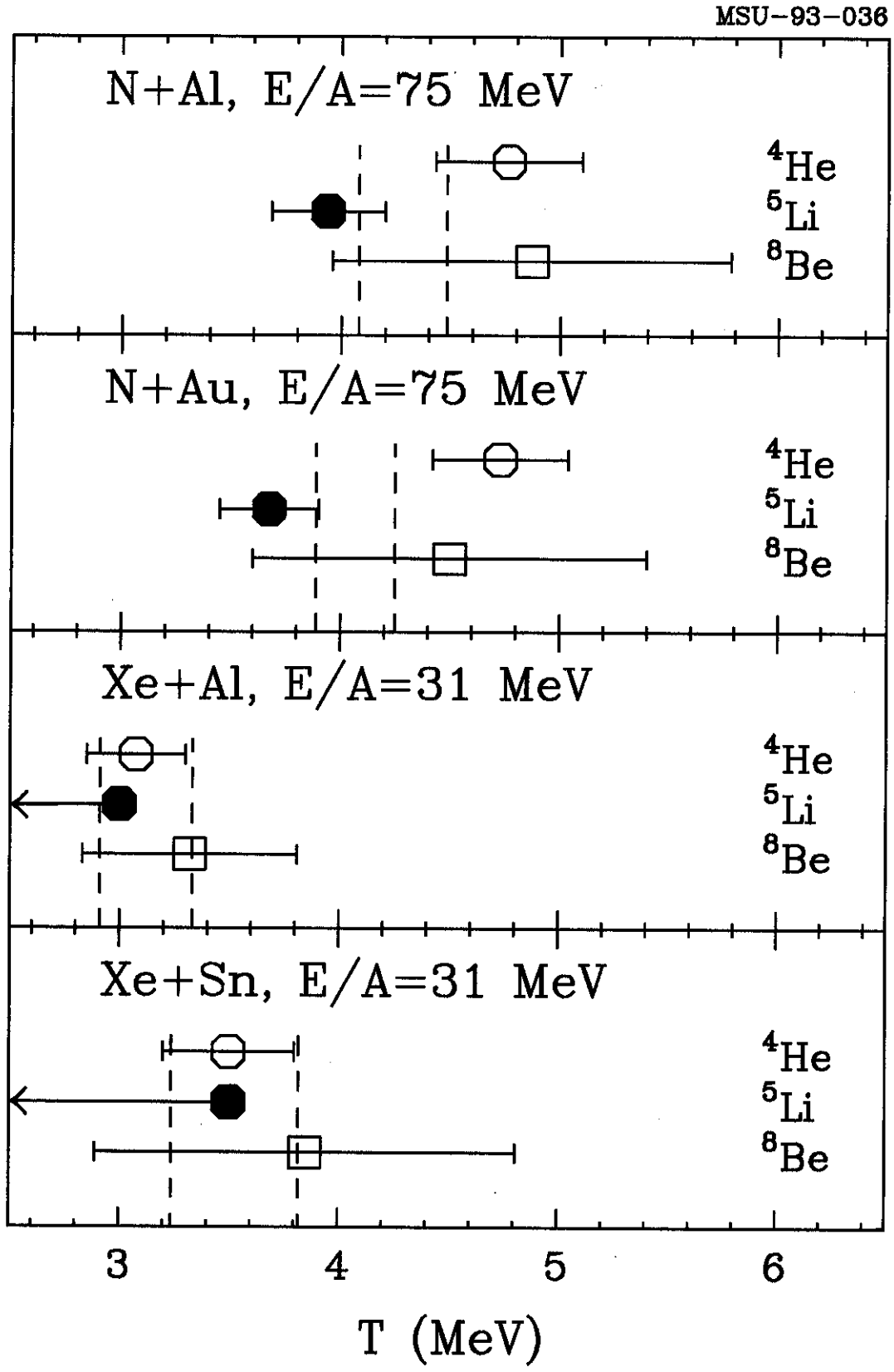
MSU-93-036
N+Al, E/A=75 MeV
N+Au, E/A=75 MeV
Xe+Al, E/A=31 MeV
Xe+Sn, E/A=31 MeV
4He
5Li
8Be
3
4
5
6
T (MeV)

Fig. 12

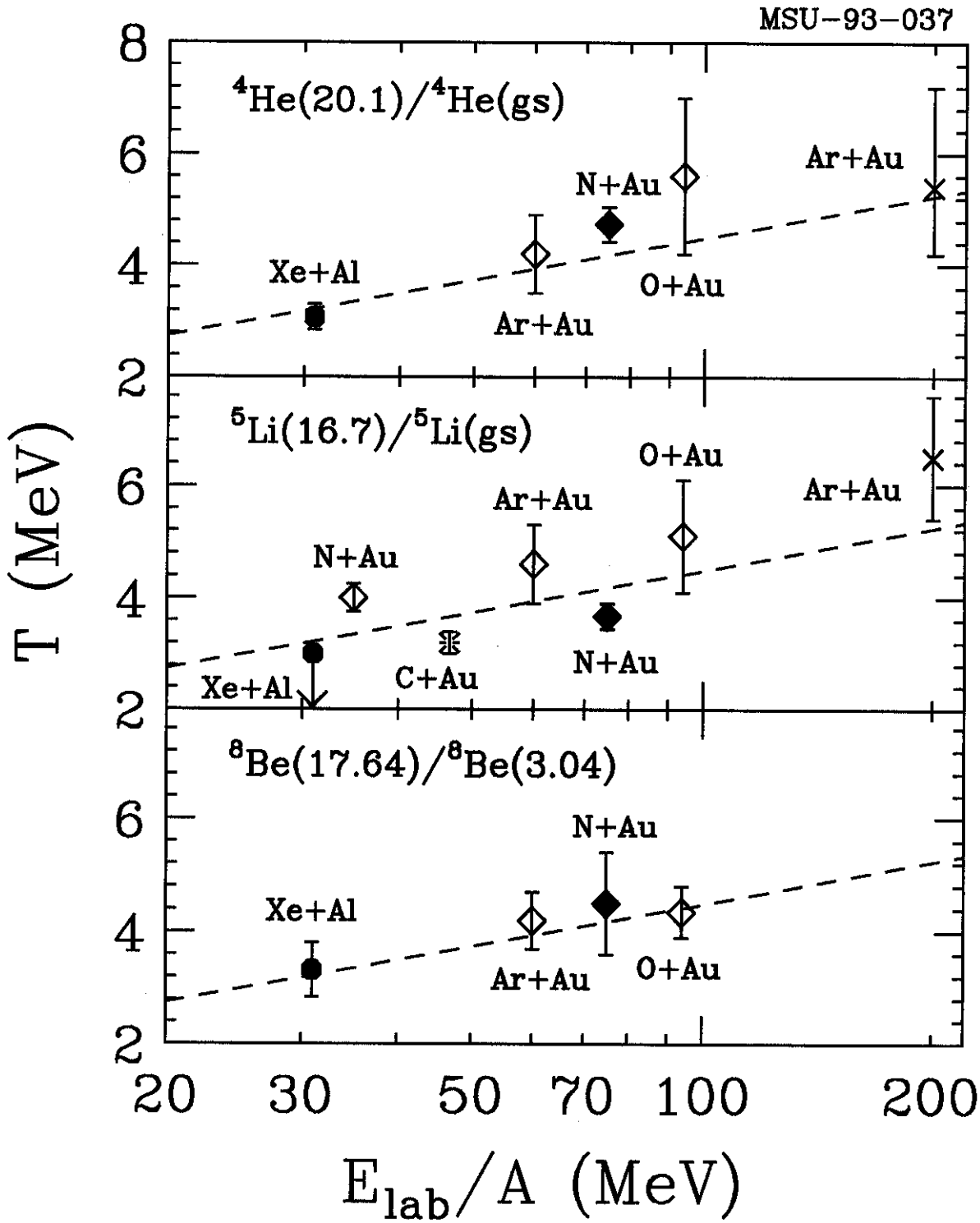
MSU-93-037
$^4$He(20.1)/$^4$He(gs)
$^5$Li(16.7)/$^5$Li(gs)
$^8$Be(17.64)/$^8$Be(3.04)
Xe+Al
Ar+Au
N+Au
O+Au
C+Au
T (MeV)
$E_{lab}$/A (MeV)
2
4
6
8
20
30
50
70
100
200

Fig. 13